FLEXIBLE PIEZOELECTRIC NANO-SENSOR FOR INFRASTRUCTURE SENSING

by

Guangshuai Han

A Thesis

Submitted to the Faculty of Purdue University

In Partial Fulfillment of the Requirements for the degree of

Master of Science in Civil Engineering

Lyles School of Civil Engineering

West Lafayette, Indiana

May 2021

THE PURDUE UNIVERSITY GRADUATE SCHOOL

STATEMENT OF COMMITTEE APPROVAL

Dr. Na Lu, Chair

School of Civil Engineering

Dr. Pablo Zavattieri

School of Civil Engineering

Dr. Tyler Tallman

School of Aeronautics and Astronautics

Approved by:

Dr. Dulcy M. Abraham

Dedicated to knowledge and exploration.

ACKNOWLEDGMENTS

Firstly, I would like to express my greatest appreciation to my advisor, Dr. Luna Lu, who has given me the continuous support and guidance thought my graduation education. Her wisdom and enthusiasm constantly excite me to dig in my research. The interaction with Dr. Lu also make my life in Purdue enjoyable. I also want to extend my appreciation to Dr. Zavattieri and Dr. Tallman for taking the time to review my thesis exam and provide valuable comments and advice.

In addition, I would like to acknowledge my colleagues from my Luna group for their wonderful collaboration. I would particularly like to single out my big bro, my friend, Mr. Yen-Fang Su. Mr. Su helped me with my research and life without any reservation.

As the type of this thesis is an article-based thesis, I would like to acknowledge the journal "ES Materials & Manufacturing", and the journal "Cement and Concrete Research" for their promptly share my work to public.

Finally, I would like to thank my parents for their everlasting encouragement throughout my life. It is the best thing that they always have my back.

TABLE OF CONTENTS

LIST OF TABLES

LIST OF FIGURES

ABSTRACT

Piezoelectric sensors have been widely used in the field of infrastructure sensing. However, the materials used for piezoelectric sensor fabrication are dominated by ceramic materials, which has the shortcoming of intrinsic brittleness. Therefore, the application of the piezoelectric sensors is limited to the condition with tiny strain levels. This study set out to develop a piezoelectric nano-sensor with good piezoelectricity and flexibility to address the current bottleneck of piezoelectric-based infrastructure sensing.

The experiment program starts from the polymer-based piezoelectric materials, PVDF (Polyvinylidene fluoride or polyvinylidene difluoride) nanofiber, synthesis by using electrospinning process. The materials characterization results reveal the correlation within the materials synthesis methods, nanostructure, and material properties. The materials synthesis techniques for nanostructure control and improve piezoelectric performance are presented in this dissertation. The piezoelectric nano-sensor was fabricated by using an ink-jet printing process. This study further utilized the COMSOL Multiphysics simulation to guide the piezoelectric nano-sensor packaging design from the perspective of energy dissipation. The optimized piezoelectric nano-sensor was then used for civil engineering materials strength sensing and damage detection. The electric response from the piezoelectric nano-sensor is sensitive to the mechanical strength of the sensing structure. The piezoelectric nano-sensor's voltage output can also be a good indicator for damage detection at a decent strain level. A natural progression of this work is to explore the roll-to-roll manufacturing methods for large-scale piezoelectric nano-sensor fabrication. As part of the infrastructure component, the piezoelectric nano-sensor is effective for the mechanical property evaluation and preliminary damage assessment. Moreover, incorporating the artificial intelligence-guided signal process, the piezoelectric nano-sensor could better understand the condition of the infrastructure.

1. APPROACHES FOR INCREASING THE B-PHASE CONCENTRATION OF ELECTROSPUN POLYVINYLIDENE FLUORIDE (PVDF) NANOFIBERS

Guangshuai Han[a], Yen-Fang Su[a], Yining Feng[a], Na Lu[a, b,c*]
[a]Lyles School of Civil Engineering, Sustainable Materials and Renewable Technology (SMART) Lab, Purdue University, Unite States
[b]School of Materials Engineering, Purdue University. Unite States
[c]Center for intelligent infrastructure, Purdue University. Unite States

Abstract

The electrospun PVDF has gained many attentions due to its excellent piezoelectricity, high flexibility, and low-cost. This study aims to develop the electrospun PVDF nanofibers with high β-phase concentration and piezoelectricity. The samples were prepared by the PVDF solution with different molecular weights. The earth abundant Zinc Oxide nanoparticles serve as the inorganic dopant to increase the polarization of the PVDF film during manufacturing process. The materials characterization methods, including Scanning Electron Microscopy, Energy Dispersive X-Ray, and Fourier-transform infrared spectroscopy were utilized to identify the material properties. The results indicate that the high molecular weight PVDF is favorable for electrospinning to obtain the high quality nanofibers. Furthermore, doping Zinc Oxide nanoparticles can effectively promote the polarization of electrospun PVDF nanofibers.

Keywords: PVDF, ZnO, Nanofiber, Electrospinning, diameter distribution, piezoelectric

1.1 Introduction

Piezoelectric materials have been widely used as actuators, sensors, transducers[1-4], and also energy harvester[5-7] due to their unique mechanical-electrical coupling properties. It was first discovered by Pierre Curie in 1880. In principle, as mechanical stress is applied to a piezoelectric material, an electrical charge appears, and vice versa due to electromechanical coupling effect. There are various types of piezoelectric materials, including ceramics, polymers, even biological matter. Among the piezoelectric materials, piezoelectric polymers have gained more attentions due to high flexibility and the potential wide range applications.

Polyvinylidene fluoride (PVDF) is the polymer-based piezoelectric materials which have attracted much interests for energy harvesting applications due to the elastic properties. It can be applied in various fields such as aerospace, civil infrastructure, and biomedical engineering, etc. The molecular structure of PVDF consists of a repetition of a monomer vinylidene fluoride unit $(-CH_2CF_2-)_n$. Among four semi-crystalline polymorphs of PVFD (α, β, γ, and δ crystalline phases), the highly polarized β-phase of PVDF has desired electroactive properties, which is favorable for energy harvesting and sensing. The polymer chains of the β-phase (in the unit cell) are arranged in a way that all the dipoles are parallel between each other, leading to a net dipole moment. Therefore, the studies on β-phase enhancement in PVDF nanofibers is of vital importance for piezoelectric applications.

The post-processes, such as mechanical stretching and corona poling, are the comment treatment to improve the β-phase content of PVDF. The stretching and corona poling process proposed by T Kaur et al. [8] have obtained the piezoelectric constant d_{31} ~60 pC/N at 30℃. A. Salimi et al. [9] suggested that stretching process can significantly improve the piezoelectric properties due to the uniform dipole moment by the orient beta phase crystals. Sencadas et al. [10] proposed using the high-temperature pressing method to eliminate the porosity of PVDF film. The results of crystallization show that this method can decrease the porosity and further improve the β-phase content of PVDF.

The electrospinning synthesis process, on the other hand, is a popular method for generating β-phase PVDF nanofibers without any post-treatment [5, 9, 11-15]. Instead of the post mechanical stretching and electrical poling, the dipoles spontaneously aligned in the electrospun nanofibers through the strong applied voltage and stretching force of the electrospinning process. The randomly oriented dipoles of α-phase will transform into β-phase which is favorable for

piezoelectric materials. Zhao et al. [11] compared the properties of electrospun PVDF with various acetone amount and DMF ratio. It has found that polymer concentration and DMF/acetone ratio were the main parameters that affected the morphology of PVDF film. Zheng et al. [16] discussed the polymorphism control of electrospun PVDF. Through adjusted the parameters such as decreasing electrospinning temperature, lower the feeding rate, and shorten the tip-to-collector distance, the β-phase of PVDF can be enhanced. Gafari et al. [15] developed a model from the experiments to predict the surface morphology and properties of PVDF nanofibers. They found that the parameters of the electrospinning process can be numerically optimized.

The PVDF film can be used as a nanogenerator for energy harvesting. The electrospun PVDF nanogenerators were found to have a high energy conversion efficiency of 5 - 2000 mV [5, 6] and the electrical output depended on the applied force and frequency. The electrospun flexible PVDF thin film has shown the potential to harvest the mechanical force under high strain conditions.

Wang et al.[12] fabricated the flexible electrospun PVDF force sensor with high sensitivity of 42 mV/N. Ghafari and Lu [4] synthesized the self-polarized electrospun PVDF sensor. They found that the PVDF device can efficiently detect the transmitted acoustic wave at the frequency range from 1 to 100 kHz.

Besides, the oxide particles such as zine oxide (ZnO) [17-28] and graphene oxide [29-35] are commonly used to improve the properties of nanomaterials including PVDF nanofibers. Among the oxides, ZnO has drawn great interest for decades owing to the versatility, environmentally friendly, earth abundancy, and excellent electrical properties. Moreover, ZnO has intrinsic wurtzite crystal structure which gives very good piezoelectric properties. Loh et al.[25] investigated the performance of ZnO nanoparticle-polyelectrolyte thin film with different ZnO weight fractions. They suggested that 50% and 60% ZnO polymer films display comparable piezoelectric properties without mechanical stretching and high-voltage poling. Ghafari et al.[23] explored the synthesis of 1D ZnO nanofibers using the sol-gel approach and electrospinning process. A parametric study on the effects of annealing temperature, annealing time, and the effect of polymer concentration were conducted while maintaining the constant electrospinning parameters such as voltage and distance between syringe and collector plate. It was found that the higher polymer concentrations produced, the larger diameter ZnO fibers; whereas higher annealing temperatures produced lower diameter fibers. Di Mauro et al.[36] investigated the synthesis of

ZnO nanofibers by electrospinning of a solution containing ZnO precursor, polyvinylpyrrolidone, and solvent. He further studied the effects of annealing temperatures and change in concentration on the electrospinning process and found that a change in concentration produced an effect on the morphology of the obtained ZnO nanofibers. Devi et al. [26] discussed the material properties of solvent casted PVDF-ZnO hybrid film. The results suggested that the ZnO has positive influence on electric and electronic properties of PVDF-ZnO composites. The stability of dispersion of particles was enhanced through surface grafting. Bafqi et al.[27] electrospun the PVDF-ZnO fibers for characterization. It has found that the film with 15 wt% ZnO can generate the output voltage up to 1.1V, which is potential for self-powered wearable devices. Dodds et al.[28] enhanced the spin coated PVDF copolymer film with ZnO nanoparticles. The results indicated that the ZnO concentration has notable effects on remnant polarization of PVDF-ZnO film. The piezoelectric ZnO nanoparticles are indeed improved the piezoelectricity of PVDF.

Owing to the excellent flexibility and process simplicity of electrospun PVDF, this study is particularly interested in synthesis PVDF nanofibers via electrospinning. Built on the knowledge of previous literatures, it has known that the parameters of electrospinning procedure and solvent concentration affect the properties of PVDF film. However, none of the studies discussed the characters of electrospun PVDF synthesized from raw PVDF ingredients with different molecular weights. Moreover, the ZnO doped PVDF nanofibers are discussed. The morphology was observed through Scanning Electron Microscopy (SEM), and the material properties were characterized using Energy Dispersive X-Ray (EDX) and Fourier-transform infrared spectroscopy (FTIR). Finally, the relationship between the PVDF parameters and β-phase crystalline was discussed.

1.2 Experiment program

1.2.1 Samples preparation

The PVDF precursor solutions were prepared by mixing the solid-state PVDF with the organic solvent. The ratio of Dimethyl sulfoxide (DMSO, Sigma-Aldrich 99.5%) and acetone (Sigma-Aldrich, 99.75%) was 7:3 for the solvent. Two types of PVDF with different molecular weights were used, including PVDF pellets (M_w=275,000, Sigma-Aldrich) and PVDF powder (M_w=534,000, Sigma-Aldrich) for comparison. To obtain high β-phase concentration and

enhanced the piezoelectricity, Zinc oxide nanoparticles (ZnO, US research Nanomaterials. Inc., diameter from 10 nm to 30 nm) was added into the PVDF precursors for electrospinning. Table 1 demonstrates the mix design for the ZnO/PVDF nanofibers.

Table 1 ZnO/PVDF nanofiber mix design

Sample	PVDF molecular weight	PVDF concentration	ZnO concentration
HW	534,000	14%	0%
HW-ZnO	534,000	14%	1%
LW	275,000	14%	0%
LW-ZnO	275,000	14%	1%

1.2.2 Electrospinning process

Electrospinning is a manufacturing method that can be used to synthesize nanofiber by applying electrostatic force to draw charged threads of polymer solutions. The electrospinning device consists of a high-voltage power source, syringe, needle and a grounded rotating collector. Figure 1 shows the set-up of the electrospinning. The prepared solution is loaded into the syringe with a needle attached. The electrical potential is applied to the needle to eject the polymer at the desired flow rate. Due to the applying of high voltage, the electrostatic force overcomes the surface tension of the polymer solution at the tip of the needle and forms a Taylor cone, which further elongates into a fluid jet. A rotating drum collects the fluid jetted fiber. The whipping motion of the polymer jet that appears between the needle and the collector allows the solvent to evaporate and remains the thin polymer film on the collector. The diameters of fibers range from the nano to the micron scale, depending on the processing parameters. Table 2 shows the parameters of the electrospinning process used by this study.

Table 2 Electrospinning parameters

Voltage	Distance between needle and collector	Flow rate	Needle
15 kV	10 cm	2 ml/h	No. 21

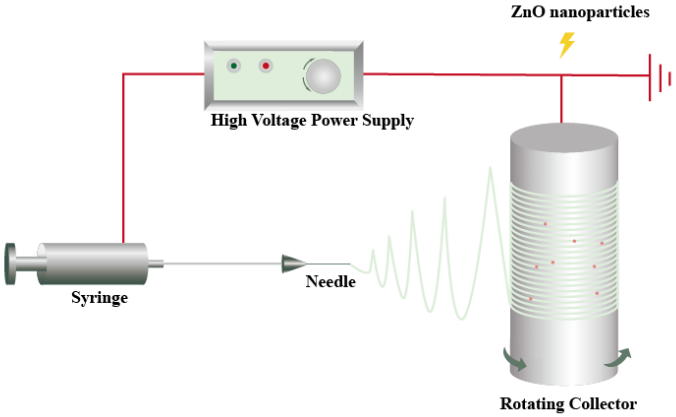

Figure 1 Schematic of the electrospinning process

1.2.3 Characterization of the samples

FTIR (PerkinElmer Spectrum 100 FTIR) spectra were employed to determine the β-phase concentration of the samples by the Spectrometer. Through FTIR analysis, molecular structure and the chemical bonding of undetermined material will be provided. Previous literature has explicated the peak locations of α and β phase PVDF on FTIR spectra [37]. The peak locations of α phase PVDF are shown at the wavelength of 531, 614, 766, 796, 870, and 970 cm^{-1}. On the other hand, the β phase PVDF is presented at 440, 470, 510, 840, and 1280 cm^{-1}. In this study, the sweeping wave numbers are range from 700 cm^{-1} to 1600cm^{-1} since the wavenumber peaks of interests are 766 cm^{-1} (α phase) and 840 cm^{-1} (β phase). The resolution for the FTIR measurement is 2 cm^{-1}.
SEM (FEI Nove Nano-SEM) images were used to investigate the morphology of the nanofibers. The samples were sputter-coated by platinum. The obtained SEM images were further post-processed by the ImageJ software. EDX characterization was also used to identify the ZnO on the nanofibers.

1.3 Results and discussion

1.3.1 FTIR results of PVDF nanofibers

FTIR is an excellent tool to quantify the β-phase concentration of the PVDF nanofibers. According to the Lambert-Beer law, the relative concentration of the β-phase in a sample can be calculated by the equation below:

$$F_\beta = \frac{A_\beta}{(K_\beta/K_\alpha)A_\alpha + A_\beta} \quad (1)$$

where F_β is the calculated β-phase concentration; A_α and A_β is the absorbance at 766 cm^{-1} and 840 cm^{-1}; K_β and K_α is the absorption coefficients correspondingly.

Figure 2 shows the FTIR spectra and the calculated the β-phase concentration of the prepared samples. The distinct peak at 840 cm^{-1} indicates that the electrospinning generates abundant β-phase PVDF. As for the PVDF nanofibers without ZnO, the high molecular weight PVDF nanofibers have higher β-phase concentrations than the nanofibers prepared by the low molecular weight PVDF. The FTIR results also indicate that adding ZnO nanoparticles increases the β-phase concentration of the PVDF nanofibers. The following SEM images were used to discuss this in details.

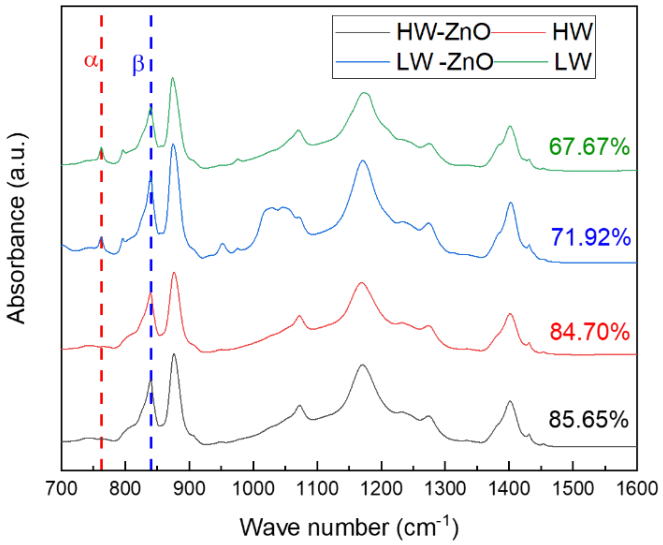

Figure 2 FTIR spectrum and β-phase concentration for different PVDF nano-fiber

1.3.2 Morphology of PVDF nanofibers

The PVDF nanofibers' diameters and beads formation are critical to the samples' performance. Figure 3 demonstrates the morphology of the PVDF/ZnO nanofibers. Based on the EDX results shown in Figure 3 (c) and (d), the ZnO nanoparticles uniformly distribute on the nanofibers. Therefore, preparing the uniform precursor solution mixed with ZnO is a feasible approach to dope ZnO nanoparticles with PVDF nanofibers. Figure 3 (a) and (b) compare the PVDF nanofibers prepared by PVDF with different molecular weights. The SEM image (on the right) for the low molecular weight PVDF nanofibers displays plenty of beads. Conversely, there are no beads in the SEM image (on the left) for the high molecular weight PVDF. The different beads formation behavior has a good agreement with the FTIR results, which PVDF nanofibers prepared by the high molecular PVDF can generate more β-phase. The molecular weight of the PVDF affects the electrospinning process by changing the viscosity of the precursor solution [38]. The product from high molecular PVDF usually has a denser structure and better mechanical performance [39, 40]. The high molecular PVDF powder is more suitable to perform the electrospinning process for high quality of PVDF nanofibers.

1.3.3 Fiber distribution PVDF/ZnO nanofibers

This section conducts the advanced analysis of the SEM images of the PVDF nanofibers. Figure 4 compares the high molecular weight PVDF nanofibers with and without ZnO. ImageJ software was utilized to perform the fiber diameter analysis. As shown in Figure 4, before adding ZnO nanoparticles, the PVDF nanofibers' diameter mainly distribute in the range from 150 nm to 200 nm. However, the fibers diameter of PVDF nanofibers with the ZnO nanoparticles tend to cluster in the range below 100 nm. The reason is that the ZnO can help the precursor solution carry more electric charges. Thus, the electric field between the needle and rotating collector can apply more electrostatic force on the ejecting solution, which is preferable to stretch the fiber during the electrospinning process. The electrospun PVDF fibers then have more polarization at the same time. Therefore, adding ZnO nanoparticles can increase the β-phase of the PVDF nanofibers.

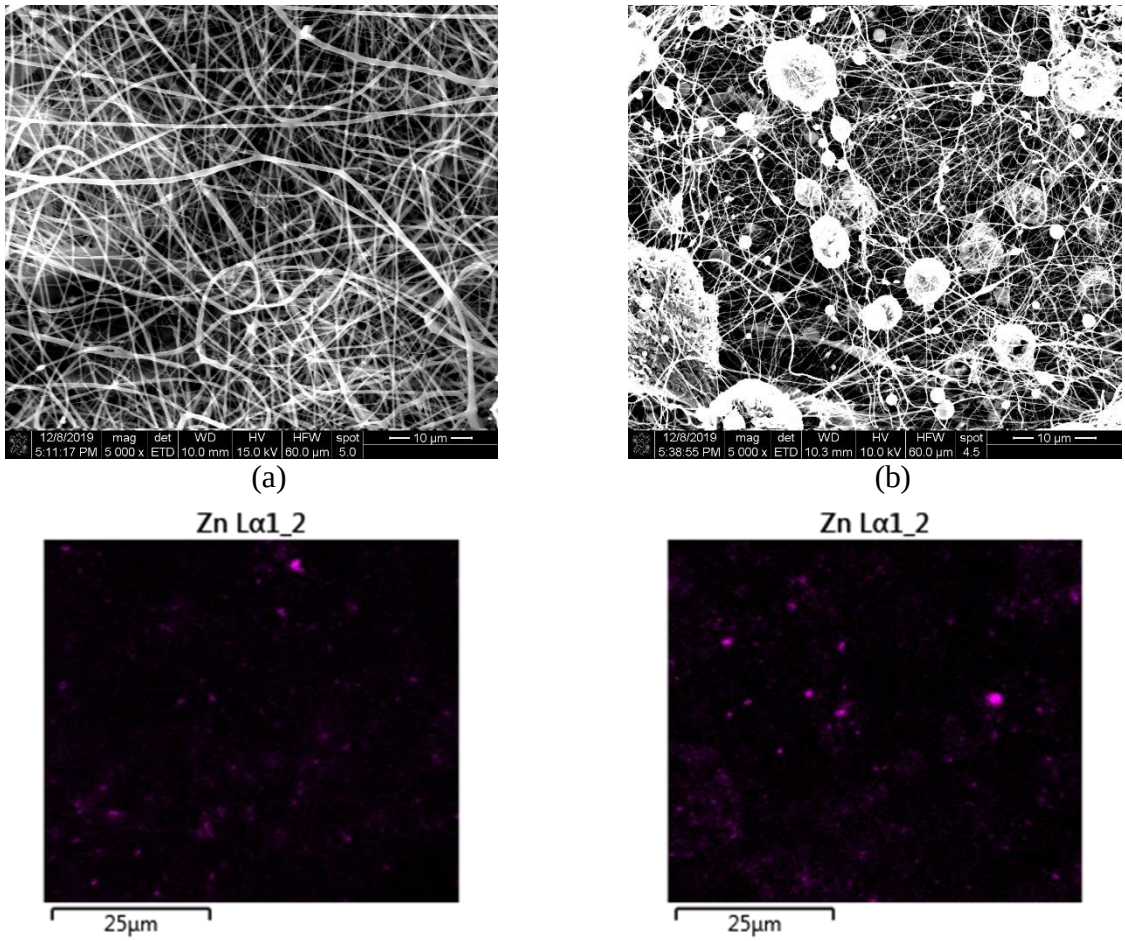

Figure 3 (a) SEM images for high molecular weight PVDF/ZnO nanofibers (HW-ZnO); (b) SEM images for low molecular weight PVDF/ZnO nanofibers (LW-ZnO); (c) EDX Zinc atom distribution for high molecular weight PVDF/ZnO nanofibers (HW-ZnO); (d) EDX Zinc atom distribution for low molecular weight PVDF/ZnO nanofibers (LW-ZnO);

Similarly, Figure 5 compares the low molecular weight PVDF nanofibers with and without ZnO nanoparticles. A finer fiber distribution is observed when adding the ZnO nanoparticles in the PVDF nanofibers. This observation meets the abovementioned findings. The FTIR result has also verified the higher polarization of the PVDF/ZnO nanofibers.

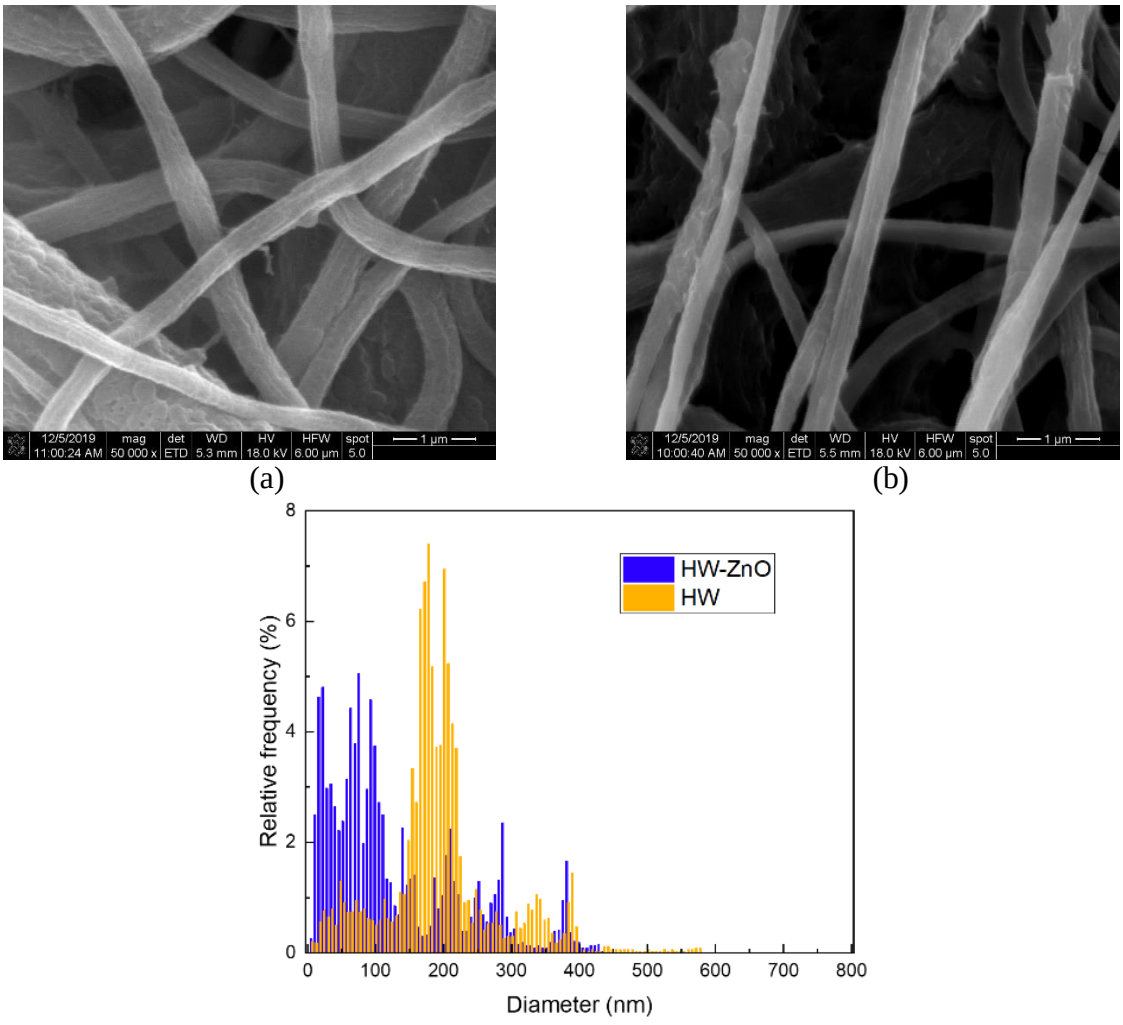

Figure 4 (a) SEM images for high molecular weight PVDF nanofibers (HW); (b) SEM images for high molecular weight PVDF/ZnO nanofibers (HW-ZnO); (c) fiber diameter distribution comparison.

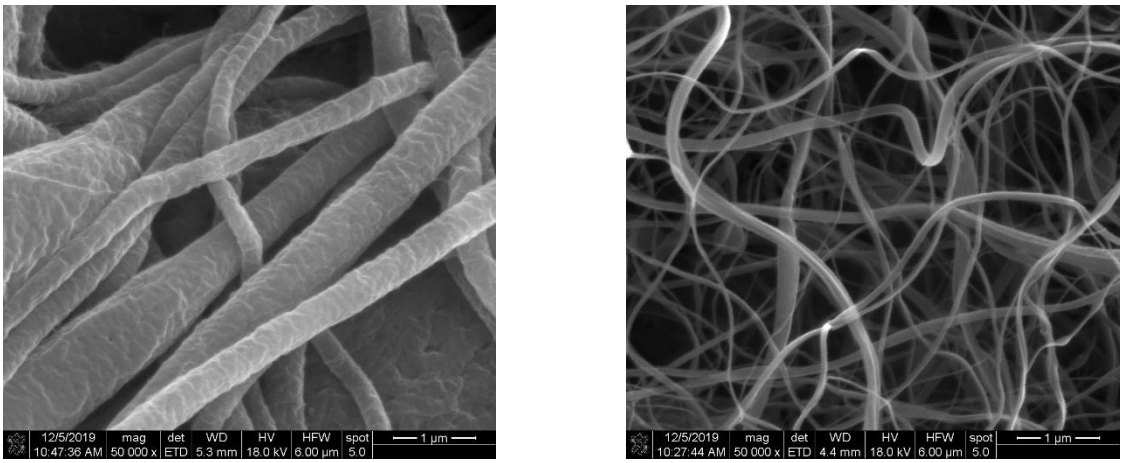

(a) (b)

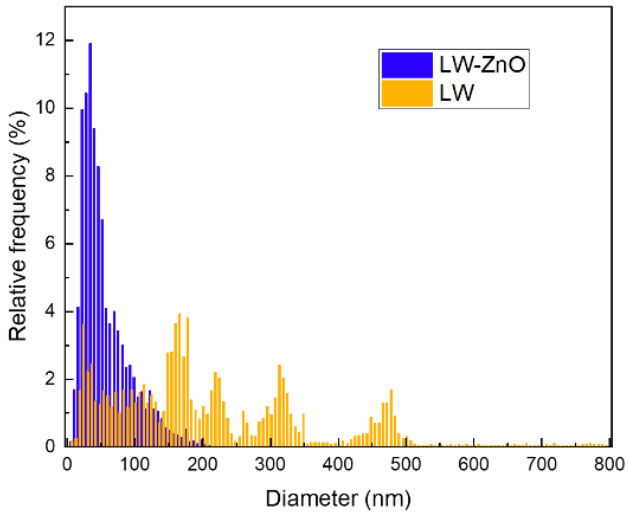

(c)

Figure 5 (a) SEM images for low molecular weight PVDF nanofibers (LW); (b) SEM images for low molecular weight PVDF/ZnO nanofibers (LW-ZnO); (c) fiber diameter distribution comparison.

1.4 Conclusion

A systematic study on enhancement of β-phase of electrospun PVDF nanofibers by different molecular weights of PVDF solution and addition of ZnO nanoparticle has been conducted and discussed. Through the obtained results, this study made a series of conclusion as follow. The electrospinning process can generate PVDF nanofibers with high β-phase concentration. Compare with the low molecular weight PVDF, the high molecular PVDF solution

is favorable the electrospinning since the high molecular PVDF nanofibers have fewer beads. Incorporation of ZnO nanoparticles can effectively increase the polarization of the electrospun PVDF nanofibers by carrying more electric charges. This process also decreases the fibers' sizes and increases the β-phase concentration of the PVDF nanofibers. In conclusion, the combination of the high molecular weight PVDF powders and ZnO nanoparticles has the strong potential to fabricate the high-quality materials for the piezoelectric device.

1.5 Acknowledgment

The authors thank Purdue Research Foundation for their generous financial support.

1.6 References

[1] Y.-F. Su, G. Han, A. Amran, T. Nantung, N. Lu, Instantaneous monitoring the early age properties of cementitious materials using PZT-based electromechanical impedance (EMI) technique, Construction and Building Materials 225 (2019) 340-347.

[2] E. Ghafari, Y. Yuan, C. Wu, T. Nantung, N. Lu, Evaluation the compressive strength of the cement paste blended with supplementary cementitious materials using a piezoelectric-based sensor, Construction and Building Materials 171 (2018) 504-510.

[3] H. Gu, G. Song, H. Dhonde, Y.L. Mo, S. Yan, Concrete early-age strength monitoring using embedded piezoelectric transducers, Smart Materials and Structures 15(6) (2006) 1837-1845.

[4] E. Ghafari, N. Lu, Self-polarized electrospun polyvinylidene fluoride (PVDF) nanofiber for sensing applications, Composites Part B: Engineering 160 (2019) 1-9.

[5] C. Chang, V.H. Tran, J. Wang, Y.K. Fuh, L. Lin, Direct-write piezoelectric polymeric nanogenerator with high energy conversion efficiency, Nano Lett 10(2) (2010) 726-31.

[6] J. Fang, X. Wang, T. Lin, Electrical power generator from randomly oriented electrospun poly(vinylidene fluoride) nanofibre membranes, Journal of Materials Chemistry 21(30) (2011) 11088.

[7] Y.-F. Su, R.R. Kotian, N. Lu, Energy harvesting potential of bendable concrete using polymer based piezoelectric generator, Composites Part B: Engineering 153 (2018) 124-129.

[8] T. Kaura, R. Nath, M.M. Perlman, Simultaneous stretching and corona poling of PVDF films, Journal of Physics D: Applied Physics 24 (1991).

[9] A. Salimi, A.A. Yousefi, Conformational changes and phase transformation mechanisms in PVDF solution-cast films, Journal of Polymer Science Part B: Polymer Physics 42(18) (2004) 8.

[10] V. Sencadas, R. Gregorio Filho, S. Lanceros-Mendez, Processing and characterization of a novel nonporous poly(vinilidene fluoride) films in the β phase, Journal of Non-Crystalline Solids 352(21-22) (2006) 2226-2229.

[11] Z. Zhao, J. Li, X. Yuan, X. Li, Y. Zhang, J. Sheng, Preparation and properties of electrospun poly(vinylidene fluoride) membranes, Journal of Applied Polymer Science 97(2) (2005) 466-474.

[12] Y.R. Wang, J.M. Zheng, G.Y. Ren, P.H. Zhang, C. Xu, A flexible piezoelectric force sensor based on PVDF fabrics, Smart Materials and Structures 20(4) (2011) 045009.

[13] J.A. Epaarachchi, B. Li, A.K.-t. Lau, J. Zheng, C. Xu, J. Leng, Silver nanowire dopant enhancing piezoelectricity of electrospun PVDF nanofiber web, 8793 (2013) 879314.

[14] Y. Liao, R. Wang, M. Tian, C. Qiu, A.G. Fane, Fabrication of polyvinylidene fluoride (PVDF) nanofiber membranes by electro-spinning for direct contact membrane distillation, Journal of Membrane Science 425-426 (2013) 30-39.

[15] E. Ghafari, X. Jiang, N. Lu, Surface morphology and beta-phase formation of single polyvinylidene fluoride (PVDF) composite nanofibers, Advanced Composites and Hybrid Materials (2017).

[16] J. Zheng, A. He, J. Li, C.C. Han, Polymorphism Control of Poly(vinylidene fluoride) through Electrospinning, Macromolecular Rapid Communications 28(22) (2007) 2159-2162.

[17] B. Kucukgok, B. Wang, A.G. Melton, N. Lu, I.T. Ferguson, Comparison of thermoelectric properties of GaN and ZnO samples, physica status solidi (c) 11(3-4) (2014) 894-897.

[18] F.H. Teherani, D.C. Look, D.J. Rogers, B. Hussain, B. Kucukgok, M.Y.A. Raja, B. Klein, N. Lu, I.T. Ferguson, Is ZnO as a universal semiconductor material an oxymoron?, 8987 (2014) 898718.

[19] E. Ghafari, S.A. Ghahari, Y. Feng, F. Severgnini, N. Lu, Effect of Zinc oxide and Al-Zinc oxide nanoparticles on the rheological properties of cement paste, Composites Part B: Engineering 105 (2016) 160-166.

[20] B. Kucukgok, B. Hussain, C. Zhou, I.T. Ferguson, N. Lu, Thermoelectric Properties of ZnO Thin Films Grown by Metal-Organic Chemical Vapor Deposition, MRS Proceedings 1805 (2015).

[21] S. Ghahari, E. Ghafari, N. Lu, Effect of ZnO nanoparticles on thermoelectric properties of cement composite for waste heat harvesting, Construction and Building Materials 146 (2017) 755-763.

[22] F.H. Teherani, D.C. Look, D.J. Rogers, C. Zhou, A. Ghods, K.L. Yunghans, V.G. Saravade, P.V. Patel, X. Jiang, B. Kucukgok, N. Lu, I. Ferguson, ZnO for solar cell and thermoelectric applications, 10105 (2017) 101051K.

[23] E. Ghafari, Y. Feng, Y. Liu, I. Ferguson, N. Lu, Investigating process-structure relations of ZnO nanofiber via electrospinning method, Composites Part B: Engineering 116 (2017) 40-45.

[24] D.J. Rogers, D.C. Look, F.H. Teherani, V.G. Saravade, I.T. Ferguson, A. Ghods, A.M. Elquist, Y. Wang, C. Zhou, N. Lu, A review of earth abundant ZnO-based materials for thermoelectric and photovoltaic applications, (2018) 53.

[25] K.J. Loh, D. Chang, Zinc oxide nanoparticle-polymeric thin films for dynamic strain sensing, Journal of Materials Science 46(1) (2010) 228-237.

[26] P.I. Devi, K. Ramachandran, Dielectric studies on hybridised PVDF–ZnO nanocomposites, Journal of Experimental Nanoscience 6(3) (2011) 281-293.

[27] M.S. Sorayani Bafqi, R. Bagherzadeh, M. Latifi, Fabrication of composite PVDF-ZnO nanofiber mats by electrospinning for energy scavenging application with enhanced efficiency, Journal of Polymer Research 22(7) (2015).

[28] J.S. Dodds, F.N. Meyers, K.J. Loh, Piezoelectric Characterization of PVDF-TrFE Thin Films Enhanced With ZnO Nanoparticles, IEEE Sensors Journal 12(6) (2012) 1889-1890.

[29] W. Deng, T. Kang, H. Liu, J. Zhang, N. Wang, N. Lu, Y. Ma, A. Umar, Z. Guo, Potassium Hydroxide Activated and Nitrogen Doped Graphene with Enhanced Supercapacitive Behavior, Science of Advanced Materials 10(7) (2018) 937-949.

[30] M. Idrees, S. Batool, J. Kong, Q. Zhuang, H. Liu, Q. Shao, N. Lu, Y. Feng, E.K. Wujcik, Q. Gao, T. Ding, R. Wei, Z. Guo, Polyborosilazane derived ceramics - Nitrogen sulfur dual doped graphene nanocomposite anode for enhanced lithium ion batteries, Electrochimica Acta 296 (2019) 925-937.

[31] Z. Zhang, J. Zhang, S. Li, J. Liu, M. Dong, Y. Li, N. Lu, S. Lei, J. Tang, J. Fan, Z. Guo, Effect of graphene liquid crystal on dielectric properties of polydimethylsiloxane nanocomposites, Composites Part B: Engineering 176 (2019) 107338.

[32] X. Gong, Y. Liu, Y. Wang, Z. Xie, Q. Dong, M. Dong, H. Liu, Q. Shao, N. Lu, V. Murugadoss, T. Ding, Z. Guo, Amino graphene oxide/dopamine modified aramid fibers: Preparation, epoxy nanocomposites and property analysis, Polymer 168 (2019) 131-137.

[33] J.-X. Zhang, Y.-X. Liang, X. Wang, H.-J. Zhou, S.-Y. Li, J. Zhang, Y. Feng, N. Lu, Q. Wang, Z. Guo, Strengthened epoxy resin with hyperbranched polyamine-ester anchored graphene oxide via novel phase transfer approach, Advanced Composites and Hybrid Materials 1(2) (2017) 300-309.

[34] M. Ataur Rahman, G.-S. Chung, Synthesis of PVDF-graphene nanocomposites and their properties, Journal of Alloys and Compounds 581 (2013) 724-730.

[35] M. Abbasipour, R. Khajavi, A.A. Yousefi, M.E. Yazdanshenas, F. Razaghian, The piezoelectric response of electrospun PVDF nanofibers with graphene oxide, graphene, and halloysite nanofillers: a comparative study, Journal of Materials Science: Materials in Electronics 28(21) (2017) 15942-15952.

[36] A. Di Mauro, M. Zimbone, M.E. Fragalà, G. Impellizzeri, Synthesis of ZnO nanofibers by the electrospinning process, Materials Science in Semiconductor Processing 42 (2016) 98-101.

[37] F. Mokhtari, M. Latifi, M. Shamshirsaz, Electrospinning/electrospray of polyvinylidene fluoride (PVDF): piezoelectric nanofibers, The Journal of The Textile Institute (2015) 1-19.

[38] Z. Chen, D. Rana, T. Matsuura, D. Meng, C.Q. Lan, Study on structure and vacuum membrane distillation performance of PVDF membranes: II. Influence of molecular weight, Chemical Engineering Journal 276 (2015) 174-184.

[39] N. Li, Z. Chang, Q. Lu, C. Xiao, J. Wu, C. Liang, Effect of the molecular weight and its distribution of polyvinylidene fluoride on the relationship between the spinning process, microstructure and properties of hollow fiber membranes via thermally induced phase separation, Textile Research Journal 89(7) (2018) 1311-1320.

[40] S. Rajabzadeh, D. Ogawa, Y. Ohmukai, Z. Zhou, T. Ishigami, H. Matsuyama, Preparation of a PVDF hollow fiber blend membrane via thermally induced phase separation (TIPS) method using new synthesized zwitterionic copolymer, Desalination and Water Treatment 54(11) (2015) 2911-2919.

2. IN-SITU RHEOLOGICAL PROPERTIES MONITORING OF CEMENTITIOUS MATERIALS THROUGH THE PIEZOELECTRIC-BASED ELECTROMECHANICAL IMPEDANCE (EMI) APPROACH

Guangshuai Han[1], Yen-Fang Su[1], Siwei Ma[1], Tommy Nantung[5], Na Lu[1,2,3,4]
[1]Lyles School of Civil Engineering, Sustainable Materials and Renewable Technology (SMART) Lab, Purdue University, 550 Stadium Mall Drive, West Lafayette, IN 47907-2051, USA
[2]Center for Intelligent Infrastructures, Purdue University
[3]School of Materials Engineering, Purdue University
[4]Birck Nanotechnology Center, Purdue University
[5]Office of Research and Development, Indiana Department of Transportation. Unite states

Abstract

More attention has focused on the elastic properties of fresh state cement-based materials due to the emergence of additive manufacturing techniques. Without the support of the conventional formworks, the shaping of the additive manufactured concrete structure mostly depends on the rheological properties of the fresh materials. Even though the fresh state cementitious materials' rheological properties can be well characterized by using a rheometer, no previous study has investigated the effective and reliable real-time monitoring methods for in-situ rheological properties monitoring. This paper attempts to investigate the feasibility of using the piezoelectric-based electromechanical impedance (EMI) method to fill this gap. The EMI tests and the rheological test was performed simultaneously. The calculated sensing index from EMI signals displays an excellent linear correlation with the results from the rheometer. The findings from this study proved that the EMI method is promising for in-situ monitoring of the fresh state cementitious materials' rheological properties.

Keywords: Piezoelectric, Additive manufacturing, Cementitious materials, Rheology.

2.1 Introduction

The cement paste is the (thixotropic) yield stress fluid at its fresh state [1], in other words, it acts as a solid-like material if the applied shear stress is lower than its yield stress. It has been reported that the fresh cementitious material can exhibit the elastic modulus as short as a few seconds after the mixing. The very early age rheological parameter and elastic modulus are very important properties for enabling many emerging technologies such as three-dimensional (3D) concrete printing technology.

3D concrete printing is an additive manufacturing technology by using concrete or mortar as the ink [2]. The fresh concrete/mortar is pumped and extruded through the nozzle and deposited layer by layer without the presence of formwork. N. Roussel [3] examined the rheological requirements for printable concretes and pointed out the importance of the elastic modulus to control the layer geometry and avoid buckling failure. It is known that some viscosity modifying agents can significantly reduce the elastic modulus of fresh state cementitious materials [4], leading to excessive deformation upon deposition, which can reach up to a few tens of centimeters for a two-meter printed wall [3]. Also, the elastic buckling failure of a freshly printed slender vertical structure has been reported in recent papers [5-7], which illustrates that the elastic modulus has to stay higher than a critical value to avoid the loss of stability.

It remains a significant challenge to accurately measure the real-time elastic modulus for the in-situ 3D concrete printing projects. Some research groups utilized the high-end rheometer to apply small-amplitude oscillation for the measurement of the elastic modulus of fresh paste, and it increases the budget for research and industrial application. The measurements obtained from different rheometers are likely different for the same material due to errors that come from the calibration [8]. Most importantly, the laboratory measurement may not reflect the “real” elastic modulus of the printed structure, especially given that the rheological properties of the cement paste vary from batch to batch, and the uncertainty can be of order 25% even the pastes have the same composition [5]. Thus, it is critical to develop an in-situ and reliable method to monitor the elastic modulus of 3D printed concrete.

The piezoelectric sensor-based electromechanical impedance (EMI) method has proven its feasibility and effectiveness for monitoring the mechanical information of structures[9-12]. It can also be used to detect the structural damage condition and monitor the in-situ mechanical properties of concrete. Owing to its high sensitivity and its direct and inverse piezometric principle,

the piezoelectric sensor can act as both sensor and actuator to capture the properties changes inside the structures. Su et al. have researched monitoring the mechanical properties of cement mortar at its very early age (4-8 hrs). The EMI results from their studies shown that the compressive strength and elastic modulus of cement mortar have high correlations with the EMI spectrum[13-15]. Tawie et al. [16] monitored the bonding development between steel rebar and concrete. It has been found that the conductance spectrum can be used to measure the change of the gradual adhesion between rebar and fresh concrete. Providakis et al. [17] used the reusable piezoelectric transducer to monitor the initial hydration states of concrete. Their results showed that the statistical indices are sensitive to concrete strength development. Narayanan et al. [18] found that the frequency shift and magnitude of the EMI results can well be correlated with material stiffness changes over time. Visalakshi et al. [19] carried out the study of using the non-dimensional parameters to track the hydration of concrete. The results indicated that the refined structural impedance parameter could eliminate the PZT contribution of hydration monitoring of concrete. Thus, the EMI method has shown its reliability for monitoring the hydration of the concrete.

Most of the studies in the piezoelectric materials-based EMI method have focused on monitoring the hydration and strength gain of the cementitious materials. There is a gap in exploring the potential of the EMI method for monitoring the rheological properties of cementitious materials. The merit of the EMI method, such as accurate, low-cost, and instantaneous, could provide great promises to evaluate the 3-D printed concrete structure's rheological properties. To fill this knowledge gap, this study served as the pilot research to examine the feasibility of using the EMI sensing method to address real-time monitoring of the rheology of cement paste. Although most of the 3D printing projects adopted concrete or mortar as the printing ink, which includes larger, inert particles compared with the plain paste, the cement paste can be considered as the active phase in these systems regarding its elastic modulus. The time evolution of the elastic modulus due to the hydration mechanism and thixotropy rebuilding are primarily dependent on the paste phase. The EMI signals from the impedance analyzer and the elastic modulus from the rheometer are tested simultaneously in this study. A linear least square regression is utilized to determine the accuracy of the EMI sensing results. The feasibility of the piezoelectric materials-based EMI method for instantaneously monitoring the elastic modulus of the fresh state cementitious is established.

2.2 Rheological measurement of cementitious materials

There are more than 100 methods developed to evaluate the rheology and workability of cementitious materials [20]. According to ACI 238 report [21], the methods can be classified as single-point tests and multi-point tests. Single point tests refer to the measurement as only standing for one point on the flow curve such as the slump test. On the other hand, the multi-point tests collected additional points for the flow curve by changing the shear rate which can constantly provide the rheological information, such as the rheometer. Another distinction of this method can be divided into a dynamic and static testing method. For dynamic methods, the instrument would transmit the energy (vibration, shear force, or jolting) into the concrete. On contrary, the static methods rely on the spontaneous gravitational force (self-weight) of concrete to flow.

To access the rheological properties of cementitious materials precisely and continuously, the rotational rheometer is typically used for the measurement. The material is sheared between two plates during the operation. The rotational speed and torque are recorded. Two types of control modes can be performed: stress-controlled and rate-controlled. The outcome of the measurement can be converted to shear rate through rotation speed and shear speed through torque if the geometry of the sample meets certain criteria. The fresh state cementitious materials have viscoelastic behavior is generally described as Bingham fluid. As such, the cementitious materials would behave their solid properties when the applied shear stress τ is lower than the yield stress τ_Y, and would present their flow properties when τ is greater than τ_Y.

In the solid regime of viscoelastic materials, the elastic modulus can be measured using a rotational rheometer with a sufficiently low strain. Another alternative approach for the elastic modulus measurement is through applying the strain oscillation as equation (1) described. The stress response $\tau(t)$ can be measured with the oscillation and be expressed as equation (2) under the linear regime [22].

$$\gamma(t) = \gamma_0 sin\omega t \quad (1)$$

$$\tau(t) = G'(\gamma_0 sin\omega t) + G"(\gamma_0 cos\omega t) \quad (2)$$

Where γ_0 is the amplitude of shear strain, G' is defined as elastic modulus, and $G"$ is defined as the viscous modulus.

To interpret the aforementioned coefficients, we can consider the simplest model for viscoelastic solid materials, which is the Kelvin-Voigt model as Figure 6 shown. The relationship between shear stress and strain is described in equation (3). Hence, the modulus G' and $G"$ is further expressed as equation (4) and (5).

$$\tau = G\gamma + \eta\dot{\gamma} \quad (3)$$

$$G'(\gamma_0, \omega) = G \quad (4)$$

$$G"(\gamma_0, \omega) = \eta\dot{\gamma} \quad (5)$$

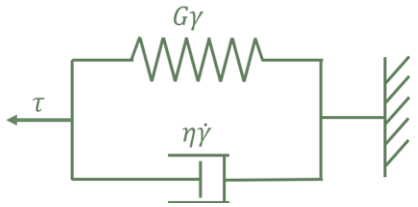

Figure 6 Kelvin-Voigt model

Build upon the concept of the theory in this session, the proposed EMI method would be the potential approach to identify the rheological properties of cement paste. This research compared the results of the commercially available rheometer with the EMI method, which both of these two methods are multi-point dynamic testing approach.

2.3 EMI principles and signal processing

The purpose of the EMI method is original to be developed for identifying the structural response subjected to the applied force. To be more specific, the response mechanical impedance of the structural system is defined as the ratio of the applied sinusoidal driving force to the consequential velocity. Liang et al. [9] developed the one-dimension model to describe the mathematical relationship between the host structure and sensor, as Figure 7 shows. A sinusoidal alternative current (AC) is applied to the sensor, which generates vibration (continuous small deformation) and transferred to the attached structure. The response of the local area is bounced back to the sensor in the form of electrical signals. Any changes in structures can be described as the combination of mass (M), spring (K), and damper (C) as shown in the model below.

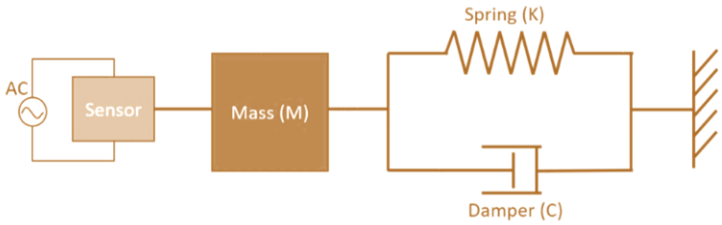

Figure 7 One-dimension model for piezoelectric sensor-driven structural dynamic system

Three parts govern the dynamic interaction between sensor and host structure, including (a) piezoelectric constitutive relation of the sensor, (b) equation of motion (EOM) for host structure and piezoelectric sensor, and (c) equilibrium and compatibility conditions of the host structure. In the EMI technique, the driving force (axisymmetric vibrations) is generated by the PZT sensor, which can be expressed as piezoelectric strain-charge form constitutive relation of the sensor as equation (6) and (7) shown.

$$S = \frac{T}{C_E} + d^T E \tag{6}$$

$$D = dT + \varepsilon_T E \tag{7}$$

where S is the strain tensor of PZT; T is the stress tensor; C_E is the elasticity matrix; d^T is the strain per unit field at constant stress; E is the applied electric field; d is the electric displacement per unit stress at the constant electric field; D is the electric displacement tensor; ε_T represents the dielectric constant. Then, the EOM for the vibrating sensor can be expressed as equation (8).

$$\rho \frac{\partial^2 u}{\partial t^2} = Y^E \frac{\partial^2 u}{\partial x^2} \tag{8}$$

Where u is the axial displacement at any point in the sensor patch, ρ is the material density. Y^E is Young's Modulus.

Lastly, considering the equilibrium and compatibility conditions of the host structure, the electrical admittance (Y, reciprocal of impedance) of the piezoelectric sensor can be expressed as the equation (9) below electromechanical coupling between the host structure and the sensor.

$$Y = G + Bj = \omega j \frac{wl}{h}\left[\epsilon_{33} - \frac{2d_{31}^2 Y^E}{(1-v)} + \frac{2d_{31}^2 Y^E}{(1-v)}\left(\frac{Z_a}{Z_a + Z_s}\right)\frac{\tan kl}{kl}\right] \quad (9)$$

Where the admittance is a function of conductance (G), susceptance (B) with its imaginary unit (j), angular frequency of excitation (ω), PZT sensor dimension (w, l, and h – width, length, and height), electrical permittivity (ε_{33}), piezoelectric coefficient (d_{31}), Poisson's ratio (v), and wavenumber (k). Except for Y, G, Z_a, and Z_s, all variables are a material property.

This work adopted the admittance signals of the piezoelectric sensor, which is able to reflect the mechanical information of the host structure, to monitor the rheology property of the very early age cementitious materials. The cumulative Root Means Square Deviation (RMSD) matrix, which has been proved as an efficient index to monitor cementitious strength gain in practical implementation [23], served as the EMI sensing index to estimate the rheology property of the host structure. The electromechanical admittance signal changes of the PZT sensor at adjacent ages indicated the gradational development of elastic modulus. Hence, the value between each adjacent EMI measurement can be calculated using equation (10).

$$Cumulative\ RMSD(k)(\%) = \sum_{1}^{k}\sqrt{\frac{\sum_1^N (Y_k - Y_{k-1})^2}{\sum_1^N (Y_{k-1})^2}} \quad (10)$$

where Y_k is the signal at curing age k, Y_{k-1} is the adjacent signal of Y_k, and N is the total number of collected data points of each signal. For example, the 20th minutes RMSD value calculates the difference of the EMI spectrum between the 10th minutes (the adjacent measurement) and 20th minutes, and so forth. Then, each value is accumulated.

2.4 Experimental program

2.4.1 Materials

Aiming to investigate the proposed rheological sensing method, two parts of experiments, namely varied mix design tests, and varied curing temperature tests were designed to evaluate its

sensing performance of the fresh state cementations materials with different mix design curing temperatures. Type I cement with water was used to prepare the cement paste. To evaluate the sensing behavior on the samples with different mix designs, the water to cement ratio varied from 0.3 to 0.6. The water to cement ratio was fixed at 0.45 when the curing temperature was varied. All the samples were prepared by hand mixing for 3 minutes due to the relatively low demand for materials. The prepared samples were then used for both the EMI test and the rheology test simultaneously to minimize the variables.

2.4.2 Testing

2.4.2.1 Sensing (EMI) Test

The prepared samples were poured into a container with a size of $50 mm^3$ right after the mixing. The polyester coated sensor, fabricated by the same procedure as ref [24, 25], was then deployed in the container's center. Each EMI test started 10 minutes after the water was added to the 160 minutes with 10 minutes interval. During the EMI test, the polyester-coated sensor was excited with a 500 mV AC voltage, with the frequency range from 5kHz to 1000 kHz. An impedance analyzer recorded the dynamic electromechanical impedance (EMI) response of the sensors. The varied mix design test was conducted in a controlled lab environment with a temperature of $23℃ \pm 2℃$. The samples for the varied curing temperature test were tested in a water bath with a temperature of 20℃, 40℃, and 60℃.

2.4.2.2 Rheology test

A rotational rheometer (Anton Paar MCR 502) with the parallel-plate measuring system was used to study cement pastes' elastic modulus. The diameter of the parallel plates is 25 mm, and the gap between the plates was selected as 1.1 mm. The sandpapers were applied to both plates to mitigate the wall slip effect. A round hood with a soaked sponge ring attached to its rim covered the parallel-plate measuring system to prevent the evaporation of the cement paste.

The testing program started immediately after loading fresh cement paste into the rheometer (10 min after water-cement contact). As the cement paste is a thixotropic material whose rheological properties depends on the shearing history, the pre-shearing at the shearing rate of 100 1/s was first applied for 60 s to ensure that all samples are at a reproducible state at the start of each test, followed by a rest for another 60 s. A small amplitude oscillatory shear (SAOS)

measurement was then employed to monitor the evolution of the elastic modulus of cement paste. Based on our previous experiences, an angular frequency of 1 Hz and a strain value of 10^{-5} were chosen for the applied strain to measure elastic storage modulus evolution.

The cement paste can be considered as a linear elastic material when the applied strain is within the range of a few 10^{-4} [26, 27], and the elastic modulus will drop dramatically, leading to a much softer material if the paste is stretched beyond the range. In the context of 3D concrete printing, we can anticipate an excessive deformation up to a few centimeters for a typical 2 m wall, which is much undesirable for the printed structure, even if the material is still at the solid regime. Thus, we focus on the elastic modulus under the strain amplitude of 10^{-5}.

2.4.2.3 Calorimetry

The isothermal calorimetry was used to measure the hydration kinetics of the cement pastes. The cement paste samples were well mixed with the same mixing speed to avoid the difference of the enthalpy. Five grams of paste were added to a glass ampoule for the measurement. The ampoules were later loaded into an isothermal calorimeter (TAM Air). The rate of hydration can be obtained by monitoring the heat flow generated under constant temperature. The testing was repeated three times and averaged to ensure consistency for each sample group.

2.5 Experimental result and discussion

2.5.1 Elastic modulus & degree of hydration

In this research, we have studied the cement pastes with different W/C ratios and curing temperatures to elucidate the feasibility of EMI as an alternative for the elastic modulus in-situ monitoring. To this end, we first measured the elastic modulus by using a rotational rheometer as a reference group. As shown in Figure 8 (a), the elastic modulus measured by the rotational rheometer appears to increase roughly linearly during the investigated age (up to 160 min) at ambient temperature, and the increasing rate accelerates with the increase of W/C ratio. It has been suggested that the elasticity of the fresh cement originate from the formation of early hydration, which is primarily calcium silicate hydrate (C-S-H) “bridges” at the contact point between cement particles [27]. Thus, the increasing rate of elastic modulus is proportional to the quantity of the C-S-H bridge at the contact point between the flocculated cement network. A. Mostafa et al. [28]

showed that the quantity of the formed C-S-H at the contact zones is proportional to the rate of rigidification; therefore, the elastic modulus is related to the hydration kinetics and the number of contacts between particles in a unit volume of paste. As shown in Figure 8 (b), the early hydration kinetics of the cement pastes are largely independent of the W/C ratio, which is in good agreement with other authors [28-30]. However, the neat cement paste with a lower W/C ratio has a higher collision frequency [28]. Therefore, the cement with a lower W/C ratio shows a higher increasing rate of elastic modulus, as seen in Figure 8 (a).

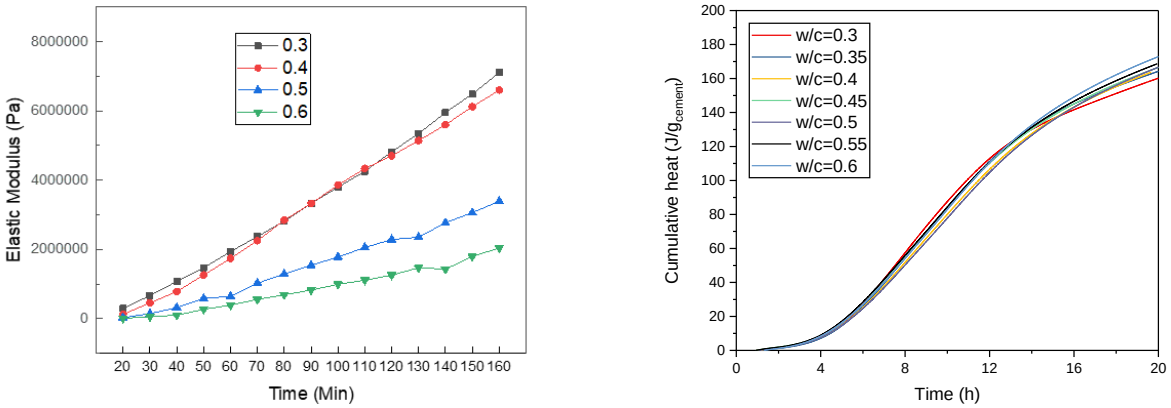

(a) (b)

Figure 8 Cement pastes with different W/C ratios. a) Elastic modulus results; b) Calorimetric results.

The temperature is also a crucial factor that will influence the increasing rate of the elastic modulus since the higher temperature can increase the collision frequency of the particles [28]. Moreover, the temperature experienced by the printed materials could be much higher than 23 ℃ due to the hot weather and heat produced by the cement hydration process in the application of 3D concrete printing. Thus, the success of monitoring elastic modules development at various temperatures is another important indicator to evaluate whether EMI can be a good alternative to rheometer. As shown in Figure 9 (a), the temperature alters the linearity of the elastic modulus evolution and significantly accelerates its rate, especially at 60 °C; it appears that the elastic modulus evolves exponentially over time.

As shown in Figure 9 (b), the elevated temperature increases the hydration rate during the investigated time range, which is in agreement with other works [31, 32]. We also noticed that the evolution of heat flow and elastic modulus share a similar pattern, which is expected as the solid

volume fraction is the same among different temperature groups; thus, the hydration kinetics could be considered as the governing factor in controlling the elastic modulus of the cement paste. Through the thermally activated process, the hydration products nucleate on the cement powder surface at a faster rate [31], leading to a faster rate of elastic modulus increase correspondingly.

To sum up, this study measured the elastic modulus development of the cement paste with different W/C ratio and curing temperature. The results have shown good agreement with other works, which are good to serve as evaluation criteria of the proposed EMI method.

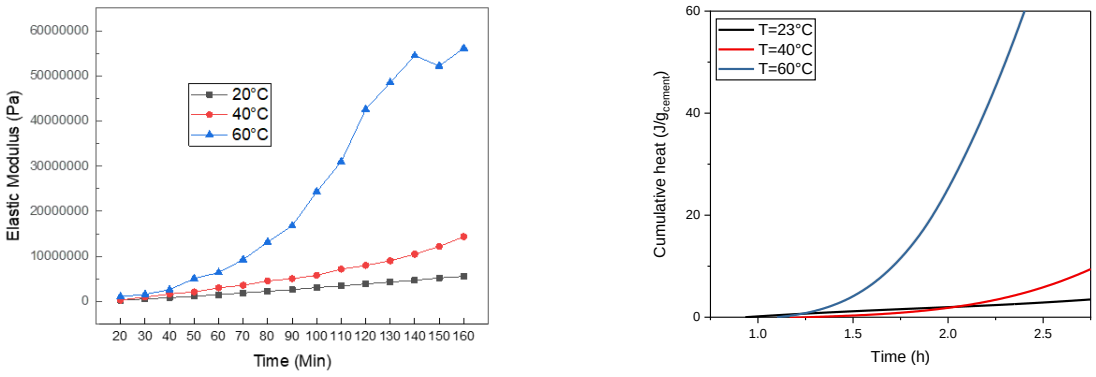

(a) (b)

Figure 9 Cement pastes with different curing temperatures. a) Elastic modulus results; b) Calorimetric results.

2.5.2 EMI sensing performance

2.5.2.1 Varied mix design test

The EMI signals of the designed four mixes were measured at each age of interest. Figure 10 plots the admittance (modulus of the reciprocal of the impedance) signals of the sensors which were embedded in the fresh state cement paste. The changes in the admittance signals of the piezoelectric sensors are always considered as the mechanical properties' changes of its host sample [33-35]. The cement paste samples curing at room temperature are in the initial reaction stage and have a slow reaction before 160 minutes, mainly resulted from the cement particle wetting, dissolution, and nucleation [36]. The samples' rheological properties change due to the formation of the C-S-H bridges. These changes are reflected by the EMI spectrum of the PZT sensor change shown in Figure 10 [37].

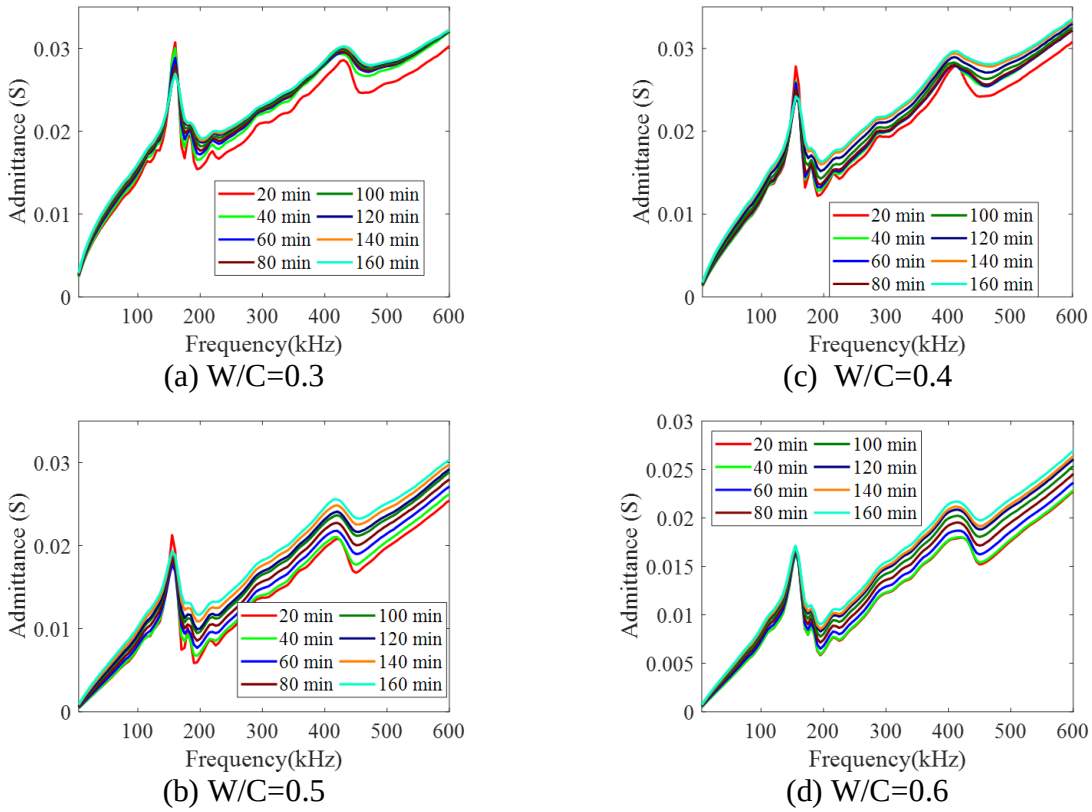

Figure 10 EMI spectrum of the sensor embedded in the cement paste with different W/C

To fulfill the mission of rheological property in-situ sensing, the EMI sensing index, calculated by the method from section 2.3, was employed as an indicator to monitor the samples' rheological properties. This study adopted the frequency range from 100 kHz to 400 kHz according to the suggestions [14] from the previous work while post-processing the EMI spectrum data. Figure 11 shows the correlation result between the EMI sensing index of the testing samples with corresponding elastic modulus. Twenty points in total were used to determine the correlation coefficient. The R-square of the sensing behavior for all mixes is above 0.91. This indicates the proposed sensing set-up with the data processing methods can be used to evaluate the rheological properties of cementitious with high accuracy.

The main reason for the high correlation between the sensing results from the piezoelectric sensor and the elastic modulus determined by the rotational rheometer is the similar strain rate during the measurement. From the discussion in section 2.3, we acknowledge that the applied strain from the rheometer to the cement paste sample is 10^{-4} to 10^{-5}. Similarly, according to the laser Doppler vibrometer results from the ref [25], the applied strain from the piezoelectric sensor

is also in the range from 10^{-4} to 10^{-5}. The small strain is crucial to obtain an accurate elastic modulus result of the cementitious sample. Thus, the proposed piezoelectric-based method can well mimic the testing mechanism of the rheometer.

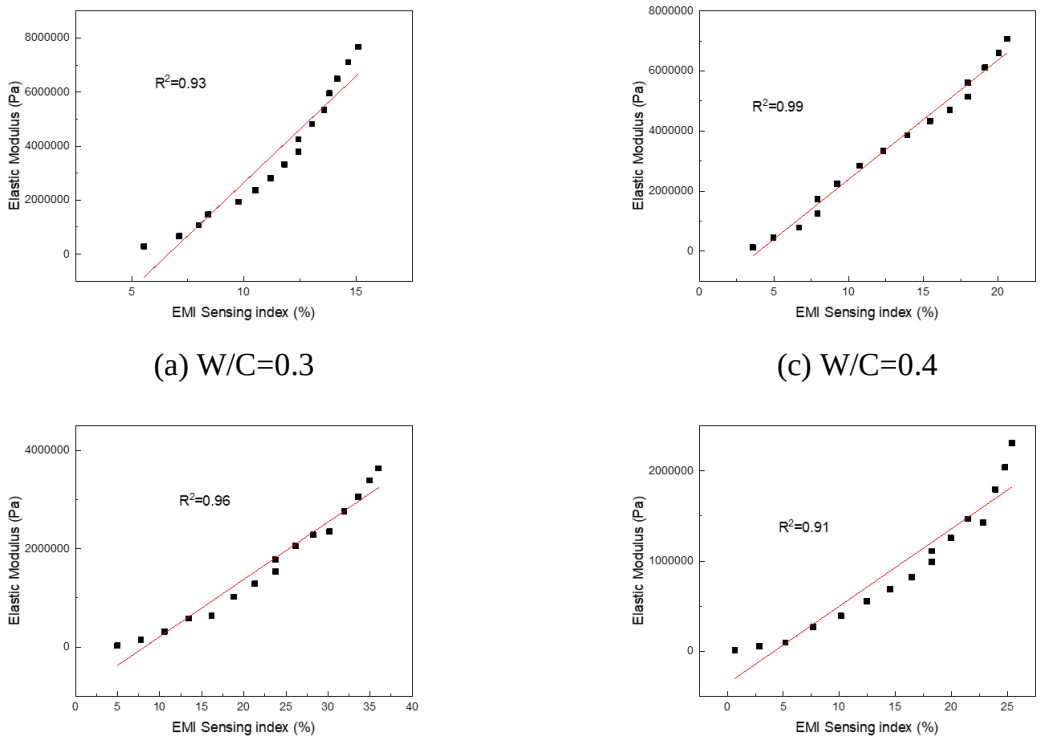

(a) W/C=0.3 (c) W/C=0.4

(b) W/C=0.5 (d) W/C=0.6

Figure 11 Linear correlation fitting between elastic modulus with EMI-RMSD index

2.5.2.2 Varied curing temperature test

The same measurement with the same data post-processing was performed on the cement paste samples with different curing temperatures. Figure 12 (a) to (c) shown the EMI spectrum change as the cement paste aged under different curing temperatures. The EMI spectrum of the samples curing at 20℃ and 40℃ changes in a similar way to the data shown in Figure 11. The trend of the EMI spectrum changes in the frequency range of interest can be characterized as an upward shift without a resonant frequency shift. It is worth noting that for the EMI spectrum of the sample curing at 60℃, a converse downward change with the resonant frequency shift showed upstarts from 120 minutes to 160 minutes. The downward shift with a resonant frequency shift of

the EMI spectrum has been reported numerous times by previous studies for using a piezoelectric sensor to monitor the hardened host structure [38-42].

Moreover, the resonant frequency in the EMI spectrum is one of the most efficient indicators for monitoring cementitious hydration and strength gaining [43-46]. Therefore, the different changing pattern of the cement paste curing at 60℃ after 120 minutes, which change to the solid phase earlier than other cement paste samples, results from the accelerated hydration speed. Differently, this study first reported the unique EMI spectrum changing pattern (Upward changing without frequency shift) when the piezoelectric sensor interacts with the cement paste in the semi-liquid phase. In this case, the resonant frequency shift is not able to monitor the elastic modulus changes at its very early age (before 120 minutes) of the cementitious material. This observation may support the hypothesis that the resonant frequency change in the EMI spectrum is the indication of the cementitious samples transit from the semi-liquid phase to the solid phase. It indicates that the cumulative RMSD is a better option when monitoring the elastic modulus monitoring at a very early age.

Figure 12 (d) to (f) demonstrates the sensing performance of the EMI sensing index calculated by the cumulative RMSD. When the cement paste subject to different curing temperatures, the speed of elastic modulus development will vary in order of magnitude due to the different hydration speeds (shown in Figure 8 and Figure 9). However, the high R-square and the identical developing trend between the EMI sensing index with the elastic modulus indicate that the proposed EMI method can monitor the very early age elastic modulus development.

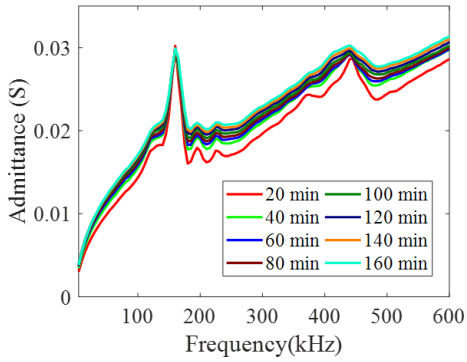

(a) EMI spectrum of cement paste curing at 20℃

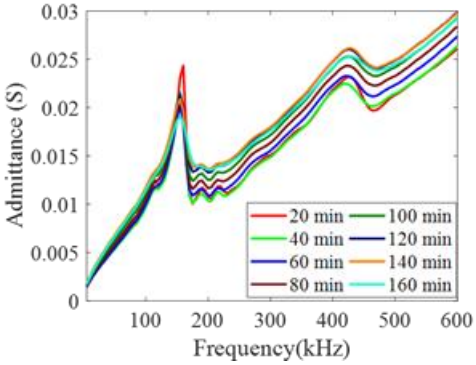

(b) EMI spectrum of cement paste curing at 40℃

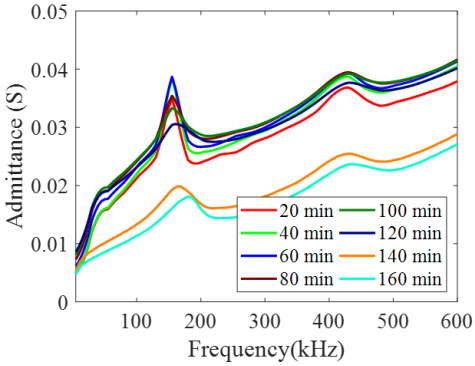

(c) EMI spectrum of cement paste curing 60℃

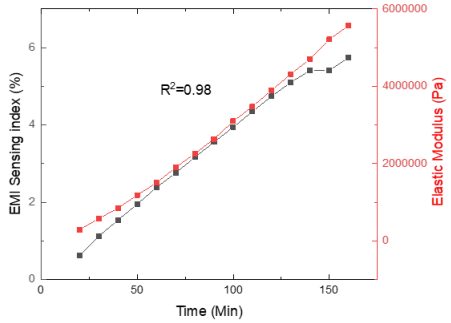

(d) Sensing index of cement paste curing at 20℃

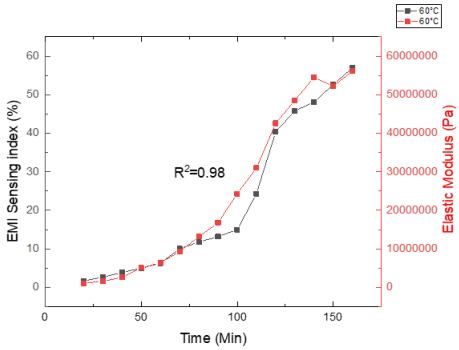

(e) Sensing index of cement paste with 40℃

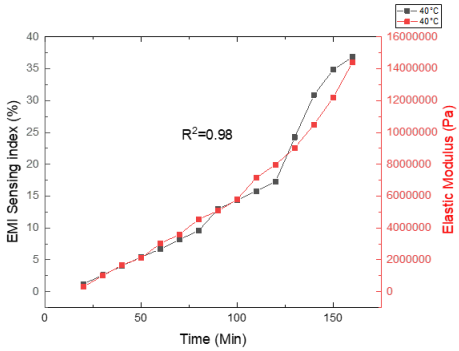

(f) Sensing index of cement paste 60℃

Figure 12 Sensing performance of the sensor embedded in the cement paste with different curing temperature

2.6 Conclusion

This study has examined the feasibility of using EMI as an in-situ sensing method for monitoring the cementitious materials' elastic modulus development for additive manufacturing. Seven sets of cement paste samples with different w/c ratios and curing temperatures were tested by EMI test, calorimetry test, and rheological test. Based on the rheological testing results, we have identified two important factors of the elastic modulus development, the water to cement ratio and the curing temperature. These two important factors could influence the elastic modulus's development via the number of contact points and the hydration kinetic. The elastic modulus results were then correlated with the piezoelectric based EMI test results. Since the EMI method provides a stable small oscillation to the cement paste, which can well mimic the testing mechanism of the rheometer, the measured elastic modulus can be estimated by the EMI test with satisfactory accuracy. The sensing index from the EMI test was based on extracting the physical information of the sample and further processed using the statistical approach. The correlation coefficients between the sensing index and the elastic modulus from the cement paste with different water to cement ratios and to cure temperature are all above 0.9. These results indicate that the proposed piezoelectric-based EMI method has a great potential to monitor the elastic modulus of the cementitious materials in a real-time manner.

Monitoring the quality and safety of the materials for additive manufacturing is always vitally important. This is the first report on providing an in-situ monitoring method for tracing the elastic modulus development of the cementitious materials, which is one of the critical properties for additive manufactured construction. The findings reported here shed new light on the in-situ monitoring technique for the burgeoning additive manufacturing. By in-situ monitoring, the elastic modulus of the cementitious materials with the proposed method, both the safety and efficiency of the additive manufacturing process can be guaranteed and strengthened. Moreover, this monitoring method can potentially be applied to similar materials systems with hardening process during the additive manufacturing process, such as heat curing, light curing, etc. Since the study is limited to the rheometer requirement, this study lacks the results of the cementitious samples with the fine aggregate and the coarse aggregate. Additionally, the samples with supplementary cementitious materials (SCMs) need to be considered. Once these mentioned factors are examined, this work could significantly contribute to monitoring of in-situ rheological properties of additive manufacturing of concrete structures.

Acknowledgments

This work is supported in part by the Joint Transportation Research Program (JTRP 4210) administered by the Indiana Department of Transportation and Purdue University, United States.

2.7 Reference

[1] F. Mahaut, S. Mokéddem, X. Chateau, N. Roussel, G. Ovarlez, Effect of coarse particle volume fraction on the yield stress and thixotropy of cementitious materials, Cement and Concrete Research, 38 (2008) 1276-1285.

[2] M.S. Khan, F. Sanchez, H. Zhou, 3-D printing of concrete: Beyond horizons, Cement and Concrete Research, 133 (2020) 106070.

[3] N. Roussel, Rheological requirements for printable concretes, Cement and Concrete Research, 112 (2018) 76-85.

[4] S. Ma, Y. Qian, S. Kawashima, Experimental and modeling study on the non-linear structural build-up of fresh cement pastes incorporating viscosity modifying admixtures, Cement and Concrete Research, 108 (2018) 1-9.

[5] R.J.M. Wolfs, F.P. Bos, T.A.M. Salet, Early age mechanical behaviour of 3D printed concrete: Numerical modelling and experimental testing, Cement and Concrete Research, 106 (2018) 103-116.

[6] R.J.M. Wolfs, F.P. Bos, T.A.M. Salet, Triaxial compression testing on early age concrete for numerical analysis of 3D concrete printing, Cement and Concrete Composites, 104 (2019) 103344.

[7] A.S.J. Suiker, R.J.M. Wolfs, S.M. Lucas, T.A.M. Salet, Elastic buckling and plastic collapse during 3D concrete printing, Cement and Concrete Research, 135 (2020) 106016.

[8] C.F. Ferraris, N.S. Martys, Relating Fresh Concrete Viscosity Measurements from Different Rheometers, Journal of research of the National Institute of Standards and Technology, 108 (2003) 229-234.

[9] C. Liang, F. Sun, C. Rogers, An impedance method for dynamic analysis of active material systems, (1994).

[10] S. Bhalla, C. Kiong Soh, Structural impedance based damage diagnosis by piezo-transducers, Earthquake Engineering & Structural Dynamics, 32 (2003) 1897-1916.

[11] Z. Kong, N. Lu, Improved Method to Determine Young’s Modulus for Concrete Cylinder Using Electromechanical Spectrum: Principle and Validation, Journal of Aerospace Engineering, 33 (2020) 04020079.

[12] R. Tawie, H.K. Lee, Piezoelectric-based non-destructive monitoring of hydration of reinforced concrete as an indicator of bond development at the steel–concrete interface, Cement and Concrete Research, 40 (2010) 1697-1703.

[13] Y.-F. Su, G. Han, T. Nantung, N. Lu, Novel methodology on direct extraction of the strength information from cementitious materials using piezo-sensor based electromechanical impedance (EMI) method, Construction and Building Materials, 259 (2020) 119848.

[14] Y.-F. Su, G. Han, A. Amran, T. Nantung, N. Lu, Instantaneous monitoring the early age properties of cementitious materials using PZT-based electromechanical impedance (EMI) technique, Construction and Building Materials, 225 (2019) 340-347.

[15] G. Han, Y.-F. Su, T. Nantung, N. Lu, Mechanism for using piezoelectric sensor to monitor strength gain process of cementitious materials with the temperature effect, Journal of Intelligent Material Systems and Structures, (2020) 1045389X20974441.

[16] R. Tawie, H.K. Lee, Piezoelectric-based non-destructive monitoring of hydration of reinforced concrete as an indicator of bond development at the steel–concrete interface, Cement and Concrete Research, 40 (2010) 7.

[17] C.P. Providakis, E.V. Liarakos, E. Kampianakis, NondestructiveWirelessMonitoring of Early-Age Concrete Strength Gain Using an Innovative Electromechanical Impedance Sensing System, Smart Materials Research, 2013 (2013) 10.

[18] A. Narayanan, A. Kocherla, K.V.L. Subramaniam, Embedded PZT Sensor for Monitoring Mechanical Impedance of Hydrating Cementitious Materials, Journal of Nondestructive Evaluation, 36 (2017).

[19] T. Visalakshi, S. Bhalla, A. Gupta, Monitoring early hydration of reinforced concrete structures using structural parameters identified by piezo sensors via electromechanical impedance technique, Mechanical Systems and Signal Processing, 99 (2018) 13.

[20] N. Roussel, Understanding the rheology of concrete, Elsevier2011.

[21] A. Commitee, 238 (2008).“Report on Measurements of Workability and Rheology of Fresh Concrete”. ACI 238-08, ACI Manual of Concrete Practice, Detroit, MI, USA.

[22] C. Derec, G. Ducouret, A. Ajdari, F. Lequeux, Aging and nonlinear rheology in suspensions of polyethylene oxide–protected silica particles, Physical Review E, 67 (2003) 061403.

[23] Y.-F. Su, G. Han, C. Huang, T. Nantung, N. Lu., Field implementation of piezoelectric sensor-based sensing technique for in-situ concrete compressive strength evaluation, ACI Materials Journal, (Under reivew) (2020).

[24] S. Yen-Fang, H. Guangshuai, A. Adlan, G. Sean Thomas, L. Na, Investigating polymer coated piezo-ceramic sensor for the very early strength monitoring of cementitious materials (Conference Presentation), Proc.SPIE, 2019.

[25] Y.-F. Su, G. Han, Z. Kong, T. Nantung, N. Lu, Embeddable Piezoelectric Sensors for Strength Gain Monitoring of Cementitious Materials: The Influence of Coating Materials, Engineered Science, 11 (2020) 66-75.

[26] S. Ma, S. Kawashima, Role of shear stress at rest on the viscoelastic response of fresh cement pastes, Journal of Rheology, 64 (2020) 433-444.

[27] N. Roussel, G. Ovarlez, S. Garrault, C. Brumaud, The origins of thixotropy of fresh cement pastes, Cement and Concrete Research, 42 (2012) 148-157.

[28] A.M. Mostafa, A. Yahia, Physico-chemical kinetics of structural build-up of neat cement-based suspensions, Cement and Concrete Research, 97 (2017) 11-27.

[29] P. Bentz Dale, A. Peltz Max, J. Winpigler, Early-Age Properties of Cement-Based Materials. II: Influence of Water-to-Cement Ratio, Journal of Materials in Civil Engineering, 21 (2009) 512-517.

[30] A.M. Ley-Hernandez, J. Lapeyre, R. Cook, A. Kumar, D. Feys, Elucidating the Effect of Water-To-Cement Ratio on the Hydration Mechanisms of Cement, ACS Omega, 3 (2018) 5092-5105.

[31] J.J. Thomas, A New Approach to Modeling the Nucleation and Growth Kinetics of Tricalcium Silicate Hydration, Journal of the American Ceramic Society, 90 (2007) 3282-3288.

[32] X. Pang, W. Cuello Jimenez, B.J. Iverson, Hydration kinetics modeling of the effect of curing temperature and pressure on the heat evolution of oil well cement, Cement and Concrete Research, 54 (2013) 69-76.

[33] Y. Yang, B.S. Divsholi, C.K. Soh, A Reusable PZT Transducer for Monitoring Initial Hydration and Structural Health of Concrete, Sensors, 10 (2010).

[34] D. Wang, H. Zhu, Monitoring of the strength gain of concrete using embedded PZT impedance transducer, Construction and Building Materials, 25 (2011) 3703-3708.

[35] D. Bahador Sabet, Y. Yaowen, Application of reusable PZT sensors for monitoring initial hydration of concrete, Proc.SPIE, 2009.

[36] J.W. Bullard, H.M. Jennings, R.A. Livingston, A. Nonat, G.W. Scherer, J.S. Schweitzer, K.L. Scrivener, J.J. Thomas, Mechanisms of cement hydration, Cement and Concrete Research, 41 (2011) 1208-1223.

[37] G. Sant, C.F. Ferraris, J. Weiss, Rheological properties of cement pastes: A discussion of structure formation and mechanical property development, Cement and Concrete Research, 38 (2008) 1286-1296.

[38] R. Tawie, H.K. Lee, Monitoring the strength development in concrete by EMI sensing technique, Construction and Building Materials, 24 (2010) 1746-1753.

[39] S.W. Shin, A.R. Qureshi, J.-Y. Lee, C.B. Yun, Piezoelectric sensor based nondestructive active monitoring of strength gain in concrete, Smart Materials and Structures, 17 (2008) 055002.

[40] Y.Y. Lim, Z.S. Tang, S.T. Smith, Piezoelectric-based monitoring of the curing of structural adhesives: a novel experimental study, Smart Materials and Structures, 28 (2018) 015016.

[41] Y.Y. Lim, K.Z. Kwong, W.Y.H. Liew, C.K. Soh, Non-destructive concrete strength evaluation using smart piezoelectric transducer—a comparative study, Smart Materials and Structures, 25 (2016) 085021.

[42] C.K. Soh, S. Bhalla, Calibration of piezo-impedance transducers for strength prediction and damage assessment of concrete, Smart Materials and Structures, 14 (2005) 671-684.

[43] D. Wang, L. Yu, H. Zhu, Strength monitoring of concrete based on embedded PZT transducer and the resonant frequency, Proceedings of the 2010 Symposium on Piezoelectricity, Acoustic Waves and Device Applications, 2010, pp. 202-205.

[44] X. Lu, Y.Y. Lim, C.K. Soh, Investigating the performance of "Smart Probe" based indirect EMI technique for strength development monitoring of cementitious materials – Modelling and parametric study, Construction and Building Materials, 172 (2018) 134-152.

[45] P. Negi, T. Chakraborty, N. Kaur, S. Bhalla, Investigations on effectiveness of embedded PZT patches at varying orientations for monitoring concrete hydration using EMI technique, Construction and Building Materials, 169 (2018) 489-498.

[46] V. Talakokula, S. Bhalla, A. Gupta, Monitoring early hydration of reinforced concrete structures using structural parameters identified by piezo sensors via electromechanical impedance technique, Mechanical Systems and Signal Processing, 99 (2018) 129-141.

3. PIEZOELECTRIC NANO-SENSOR FOR INFRASTRUCTURE SENSING

Guangshuai Han[1], Na Lu[1,2,3,4]
[1]Lyles School of Civil Engineering, Sustainable Materials and Renewable Technology (SMART) Lab, Purdue University, 550 Stadium Mall Drive, West Lafayette, IN 47907-2051, USA
[3]Center for Intelligent Infrastructures, Purdue University
[3]School of Materials Engineering, Purdue University
[4]Birck Nanotechnology Center, Purdue University

Abstract

Piezoelectric sensors have been widely used in the field of infrastructure sensing. However, the materials used for piezoelectric sensor fabrication are dominated by ceramic materials, which has the shortcoming of intrinsic brittleness. This study set out to develop a piezoelectric nano-sensor with good piezoelectricity and flexibility to address the current bottleneck of piezoelectric-based infrastructure sensing. The experiment program starts from the polymer-based piezoelectric materials, PVDF (Polyvinylidene fluoride or polyvinylidene difluoride) nanofiber, synthesized by using an electrospinning process. The materials characterization results reveal the correlation within the materials synthesis methods, nanostructure, and material properties. The piezoelectric nano-sensor was fabricated by using an ink-jet printing process. The optimized piezoelectric nano-sensor was then used for civil engineering materials strength sensing and damage detection. The electric response from the piezoelectric nano-sensor is sensitive to the mechanical strength of the sensing structure. The piezoelectric nano-sensor's voltage output can also be a good indicator for damage detection at a decent strain level.

Keywords: Piezoelectric, Infrastructure sensing, materials characterization, Ink-jet printing

3.1 Introduction

Concrete structures have been used extensively in the civil engineering field. However, compared with metallic or other composite structures, the non-destructive evaluation (NDE) technologies of concrete structures are relatively unadvanced [1]. It is urgent to build a reliable and accurate real-time monitoring and sensing system for concrete structures [2-4]. Piezoelectric materials are the most used materials for infrastructure sensing and monitoring [5]. Owing to its high sensitivity and direct and inverse piezometric principle, the piezoelectric sensor can act as both a sensor and actuator to capture the properties' changes inside the structures [6-8]. The unreadable mechanical information can be directly converted to readable digital signals. Therefore, developing good piezoelectric is essential for the development of infrastructure sensing.

The materials for piezoelectric sensor and transducer fabrication are dominated by ceramic-based materials, such as lead zirconate titanate, barium titanate, etc. However, ceramic-based materials have the shortcoming of intrinsic brittleness[9]. The application of the ceramic-based piezoelectric sensor and transducer is limited to a slight strain level. As such, this work spends effort on fabricating the piezoelectric sensor with both good piezoelectricity and flexibility to address the abovementioned problem. The polymer-based materials polyvinylidene fluoride (PVDF) with high β-phase concentration is selected as an alternative material for piezoelectric sensor fabrication [10-12]. PVDF exists in different phases, such as α-phase, β-phase, and γ-phase [12, 13]. Among all the different PVDF phases, the β-phase PVDF is considered to have the most outstanding piezoelectric properties due to the well-aligned polar structure [14, 15]. Therefore, great efforts have been made to improve the β-phase concentration of the PVDF-based piezoelectric materials. Mechanical stretching is a helpful approach for PVDF β-phase enhancement [16-19]. By external mechanical force, the PVDF polymer chain will be aligned in one direction, and the β-phase PVDF was then formed. However, the mechanical stretched PVDF has an inconsistent phase distribution. The PVDF with β-phase tends to cluster in the middle of the sample [16], which will affect the quality of the materials and device. Another approach for β-phase enhancement is electric poling. Take the electrospinning synthesis approach as an example, the PVDF polymer chain can be stretched by the applied electric field. Ghafari et al. compare the fraction of β-phase PVDF from the sol-gel process with and without electric poling process [20]. The results show that the electrospun PVDF can have a β-phase concentration of 75% with an increment up to 41%. Moreover, doping graphene oxides by co-axial electrospinning can further

improve the β-phase concentration of the PVDF [20]. The π bond of the graphene with the fluorine atoms aligns the PVDF polymer chain in one direction during the electrospinning process. Similar techniques are also verified to have significant assistance for the PVDF β-phase enhancement. Doping the 2-dimension structured materials, such as graphene and barium titanate, can increase the fraction of β-phase higher than 90% [21-25]. However, this dopant is normally having a considerable cost, which is not suitable for civil engineering applications. Therefore, this study set out to develop piezoelectric nano-sensor fabrication by using a cost-efficient approach. The detailed materials synthesis approach, device fabrication methods, and sensor sensing performance are discussed in the following section.

3.2 Experimental program

3.2.1 Materials

This study used the sol-gel electrospinning process to synthesis the materials for piezoelectric nano-sensor fabrication. The precursor solution was prepared by mixing the PVDF powder (Mw=534,000, Sigma-Aldrich) with the organic solvent. The solvent contains Dimethyl sulfoxide (DMSO, Sigma-Aldrich 99.5%) and acetone (Sigma-Aldrich, 99.75%) in a weight ratio of 7:3. The PVDF weight concentration of the precursor solutions is 8%, 10%, 12%, and 14%. The solution ingredients were then mixed together for 4 hours at room temperature by a magnetic stirrer. The viscosity measurement of different precursor solutions was performed right before the electrospinning process.

3.2.2 Electrospinning

The prepared solution was loaded into the syringe with a needle attached. During the electrospinning process, the electric field between the needle and materials collector is 1.5kV/cm. The electric field ejected the precursor solutions with a flow rate of 2 ml/h. The electrospun PVDF was collected after 3 hours.

3.2.3 Piezoelectric nano-sensor fabrication

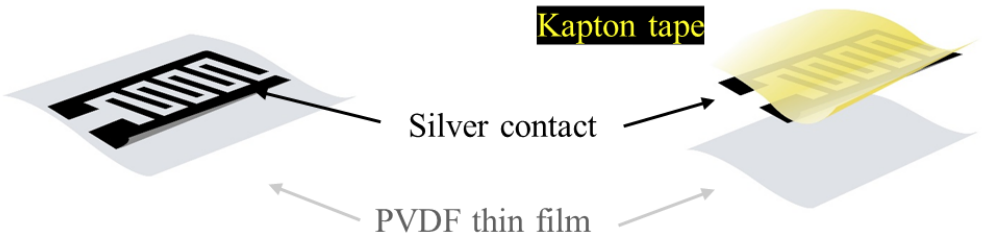

Figure 13 The contact design of the piezoelectric nano-sensor

The sensor fabrication adopted ink-jet printing for making contact with the sensor. Figure 13 shows the contact pattern of the piezoelectric nano-sensor. For the most piezoelectric nanogenerator, the contact is printed on a flexible thin film and then attached with the flexible piezoelectric materials. However, the different elastic properties and thermal expansion coefficients may induce undesirable friction, which may reduce the piezoelectric sensor/nanogenerator's durability. Therefore, this work firstly printed the silver contact directly on the PVDF thin film. For comparison, the silver ink was also indirectly printed on a Kapton tape then attached with the PVDF thin film. Since the electrospun PVDF is a porous material, printing the silver contact into two sides has a high possibility of having a short-circuit issue. Therefore, the interdigital pattern design was utilized. The piezoelectric nano-sensor fabrication was ended up with polymer coating by using Polydimethylsiloxane (PDMS).

3.2.4 nano-sensor for strength sensing

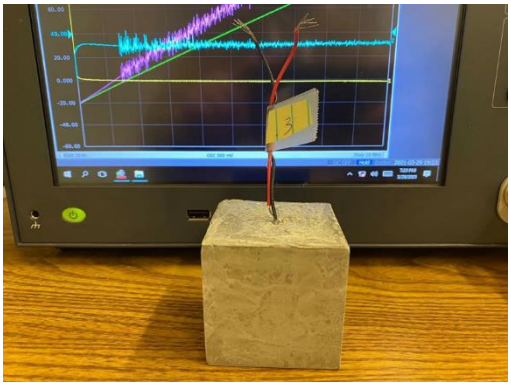

(a)

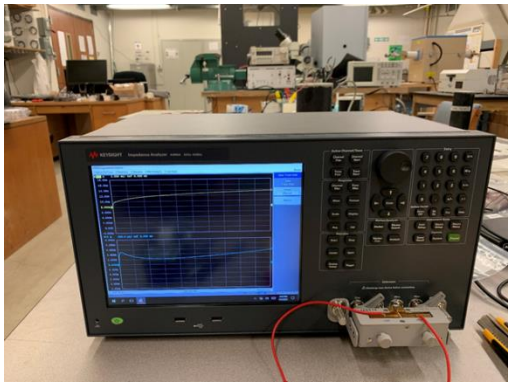

(b)

Figure 14 (a) Cement paste sample with embedded piezoelectric nano-sensor. (b) Keysight E4990A impedance analyzer.

The cement paste with different water to cement ratio 0.38, 0.40, and 0.42 was prepared to investigate the piezoelectric nano-sensor's sensing performance. We embedded the piezoelectric nano-sensor right after the mixing process. The impedance analyzer (as shown in Figure 14 (b)) excites the piezoelectric nano-sensor with a sinusoidal AC voltage at the frequency range of 1 kHz to 1000 kHz. Then, the electrical signal, conductance, and capacitance were collected at the age of 10 hours, 11 hours, 12 hours, 1 day, 3 days, and 7 days by Keysight E4990A impedance analyzer (as shown in Figure 14 (b)). Simultaneously, the cement paste sample's compressive strength was measured per ASTM C 109 at the same age for comparison. The conductance, which is the real part of the piezoelectric nano-sensor's admittance, has shown great sensitivity to the strength of the sensing structure (cement paste sample in our case) based on the previous study [4]. The equation below demonstrates electromechanical coupling between the piezoelectric sensor with the sensing structure:

$$Y = G + Bj = 4w\frac{l^2}{h}\left[\epsilon_{33} - \frac{2d_{31}^2 Y^E}{(1-v)} + \frac{2d_{31}^2 Y^E}{(1-v)}\left(\frac{Z_a}{Z_a + Z_s}\right)\frac{\tan kl}{kl}\right] \quad (1)$$

Where the admittance is a combination of real part conductance (G), imaginary part susceptance (B). The admittance depends on the PZT sensor dimension (w, l, and h – width, length, and height), electrical permittivity (ε_{33}), piezoelectric coefficient (d_{31}), Young's Modulus (Y^E), Poisson's ratio

(v), and wavenumber (k). The mechanical impedance of the piezoelectric nano-sensor (Z_a), and the mechanical impedance of the sensing structure (Z_s). Using the electromechanical impedance approach, the mechanical properties of the sensing structure can be well described by the electrical response of the piezoelectric nano-sensor. This study utilized the root mean square deviation (RMSD) sensing index (EMI-RMSD index) to correlate with the cement paste sample's strength. The equation is shown below:

$$RMSD\,(\%) = \sqrt{\frac{\sum_{i=1}^{N}(G_i - G_{bl})^2}{\sum_{i=1}^{N}(G_{bl})^2}} \qquad (2)$$

Where G_i is the conductance spectra of different curing age, G_{bl} is the baseline conductance spectra which come from the electrical measurement from the pure piezoelectric nano-sensor, N signifies the number of data points in the EMI spectra (depends on the frequency range and sampling rate).

3.2.5 Piezoelectric nano-sensor for damage detection

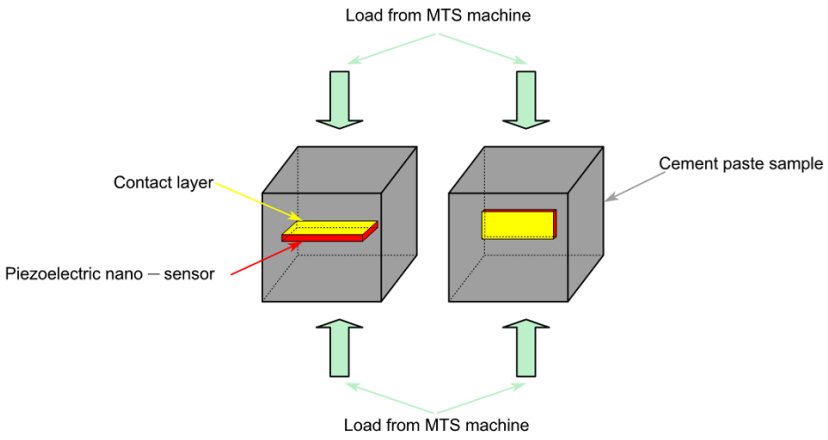

Figure 15 the schematic of the damage detection experimental setup

At the age of 7 days, the cement paste sample with embedded piezoelectric nano-sensor was broken by the compression load from the MTS machine. As shown in Figure 15, the compression load was applied in two different directions: parallel the contact surface of the

piezoelectric nano-sensor and vertical to the piezoelectric nano-sensor's contact surface. The voltage output was recorded by data logger. The stress-time was also recorded at the same time.

3.3 Materials and device characterization

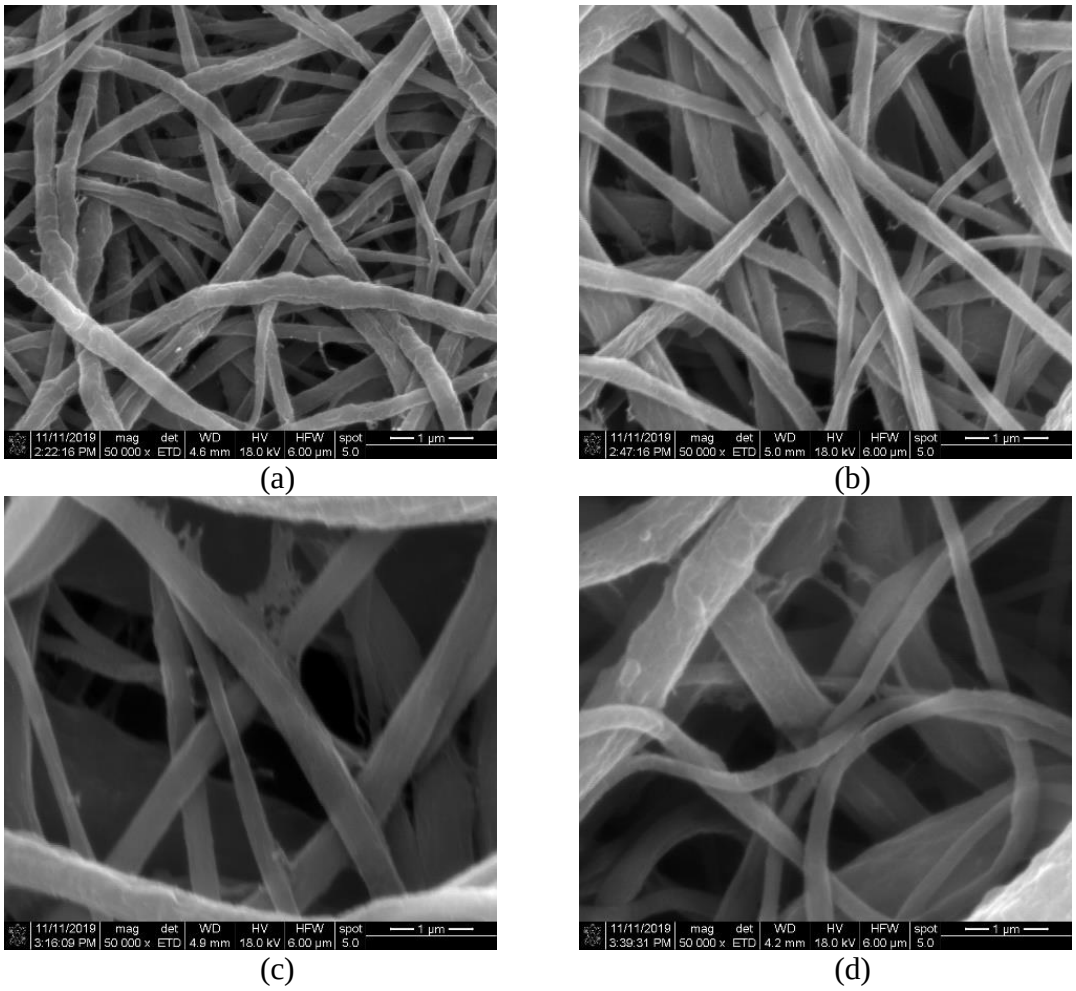

Figure 16 SEM images of electrospun PVDF nanofiber with different precursor solution (a) 8%, (b) 10%, (c) 12%, (d) 14%.

Figure 16 shows the SEM (scanning electron microscopy) image of the electrospun PVDF prepared from the precursor solution with different PVDF weight ratios. The SEM characterization identifies the fibrous nanostructure of the electrospun PVDF. The fiber diameter was analyzed by ImageJ software. As the PVDF concentration weight ratio increased, the fiber size increased (as shown in Figure 17). As such, the β-phase PVDF concentration will be increased. This observation

was verified by the FTIR (Fourier-transform infrared spectroscopy) characterization from Figure 18. The electrospun PVDF prepared by the precursor with a PVDF weight ratio 10% has the highest β-phase concentration, 87.66%. As the precursor solutions' viscosity increased, the PVDF

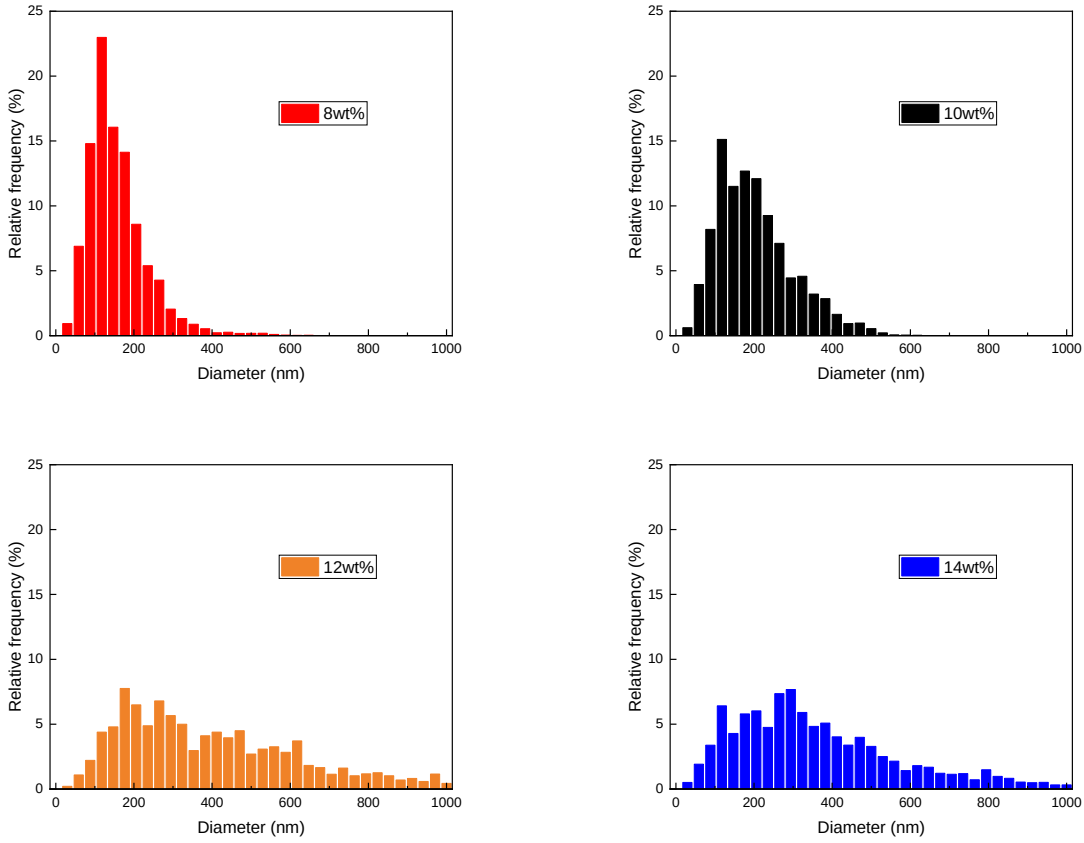

Figure 17 Nano-fiber's diameter distribution of electrospun PVDF nanofiber with different precursor solution

weight percentage increased. The precursor solutions with a lower viscosity will result in a higher β-phase concentration of the final electrospun PVDF. However, the solutions viscosity is still required to pass a sufficient criterion to maintain the Taylor cone formation. The recommended precursor solution viscosity is 200 cP for achieving the electrospun PVDF with high β-phase concentration.

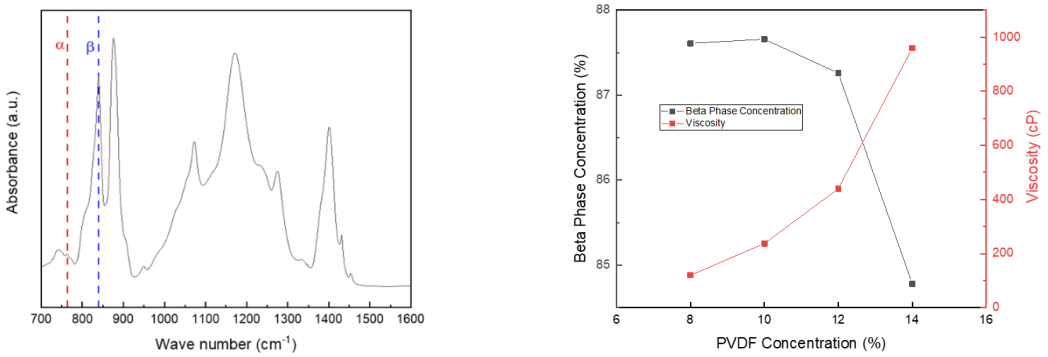

Figure 18 (a) FTIR spectrum of the electrospun PVDF nanofiber with 10% PVDF precursor solution; (b) The relationship between the precursor viscosity & the Beta phase concentration

The electrospun with the highest β-phase concentration was used to fabricate the piezoelectric nano-sensor. The mechanical vibration was applied on the fabricated piezoelectric nano-sensor by a vibration generator. The datalogger then measured the voltage output. As shown in Figure 19, the nanogenerator with direct contact can harvest more energy than the nanogenerator with the indirect contact design. The maximum voltage of the direct contact is more than 300 microvolts. It can be concluded that directly print the silver contact on the electrospun PVDF can increase the piezoelectric nano-sensor's efficiency. The piezoelectric nano-sensor was then used for strength sensing and damage detection.

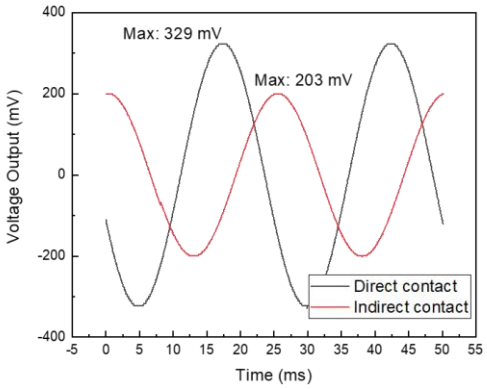

Figure 19 Voltage output measurement of the piezoelectric nano-sensor

3.4 Piezoelectric sensing performance

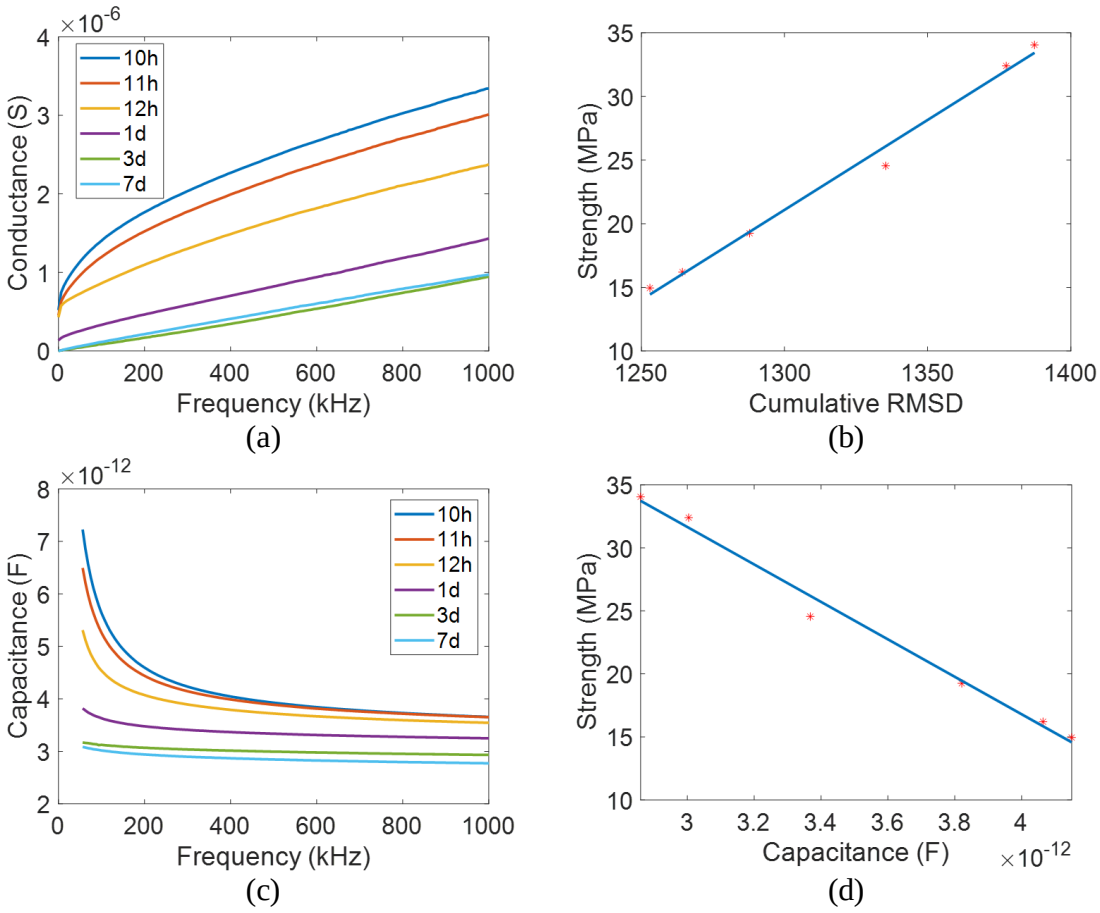

Figure 20 (a) the conductance spectrum of the embedded piezoelectric nano-sensor at different cement paste curing age; (b) The linear regression Linear correlation fitting between elastic modulus with EMI-RMSD index; (c) the capacitance spectrum of the embedded piezoelectric nano-sensor at different cement paste curing age; (d) The linear regression Linear correlation fitting between elastic modulus with average capacitance;

Figure 20 demonstrates the strength sensing performance of the piezoelectric nano-sensor which was embedded in the cement paste sample with 0.38 water to cement ratio. Figure 20 (a) plots the conductance spectrum of the embedded piezoelectric nano-sensor at different testing ages. The conductance has a downward change as the cement paste aged. Figure 20 (b) displays the correlation result between the RMSD index of the representative sample (W/C=0.38) with corresponding compressive strength at each age. This denotes that the EMI-RMSD can extract the mechanical properties of cementitious materials with reliable accuracy. As piezoelectric materials are always a good dielectric material, capacitance has also been investigated as a potential indicator

for strength sensing. Due to the PVDF nanofiber is porous material, the nanostructure and surface area of the PVDF nanofiber will be affected as the cementitious samples aged. This changed can be reflected by the capacitance of the piezoelectric nano-sensor. A high r-square was also obtained between the average capacitance and the compressive strength at different ages (as shown in Figure 20 (c) and (d)). Table 3 summarized the overall sensing performance of the cement paste sample with different water to cement ratios. A high r-square between the sensing index and samples' compressive strength was obtained.

Table 3 overall sensing performance of the cement paste sample with different water to cement ratio.

Water to cement ratio	Cumulative RMSD from conductance	Average capacitance
0.38	R^2=0.99	R^2=0.99
0.40	R^2=0.98	R^2=0.71
0.42	R^2=0.88	R^2=0.88

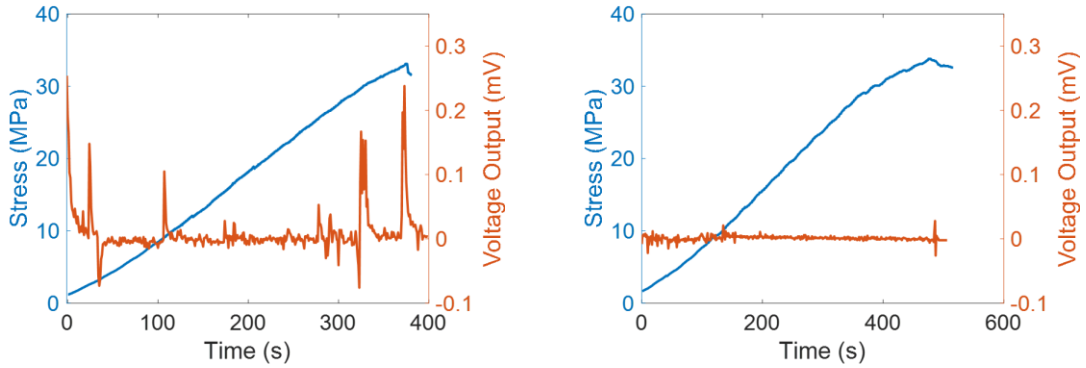

(a) (b)

Figure 21 the stress-time curve and voltage output curve of the samples tested under compression load.

The piezoelectric nano-sensor has also been used for damage detection. The cement paste with embedded piezoelectric nano-sensor was tested by compression load. Since the external mechanical stimuli of the piezoelectric materials can generate voltage [4]. The output voltage is considered a good indicator when damage appears. A distinct voltage at the peak load was observed. The piezoelectric nano-sensor placed vertically to the load direction is more sensitive to

the cement paste sample's damage. The conclusion is that the fabricated piezoelectric nano-sensor could be used for damage detection for infrastructure.

3.5 Conclusion

This study presented a comprehensive research on the infrastructure sensing potential of the self-developed flexible piezoelectric sensor. Starts from the flexible piezoelectric materials synthesis, the β-phase concentration of PVDF nanofiber has a strong relationship with the precursor solution's PVDF weight ratio. The PVDF nanofiber comes from the precursor solution with a 10% weight ratio has a finer fiber diameter and uniform fiber size distribution. In addition, the viscosity of the precursor solution is negatively related the β-phase concentration of PVDF nanofiber. For the piezoelectric nano-sensor fabrication, the newly proposed direct contact printing approach can enhance the piezoelectric nano-sensor's efficiency. The developed piezoelectric was also embedded into the cement paste sample with different water to cement ratios. The extracted sensing index from the piezoelectric nano-sensor correlates with the cement paste sample's compressive strength. Besides, the voltage output from the piezoelectric nano-sensor could be a useful indicator for damage detection.

In conclusion, the piezoelectric nano-sensor with good flexibility and piezoelectricity could be a durable sensing component for infrastructure sensing. The future work could be exploring the roll-to-roll manufacturing techniques for large-scale applications. The durable, flexible, and sensitive piezoelectric nano-sensor could be powerful equipment for infrastructure sensing. The piezoelectric nano-sensor's diverse electrical response could also incorporate with the artificial intelligence guided signal processing to better understand the infrastructure's condition.

Acknowledgments

This work is supported in part by the Joint Transportation Research Program (JTRP 4210) administered by the Indiana Department of Transportation and Purdue University, United States.

3.6 Reference

[1] S. Park, S. Ahmad, C.B. Yun, Y. Roh, Multiple Crack Detection of Concrete Structures Using Impedance-based Structural Health Monitoring Techniques, Experimental Mechanics, 46 (2006) 609-618.

[2] Y.-F. Su, G. Han, Z. Kong, T. Nantung, N. Lu, Embeddable Piezoelectric Sensors for Strength Gain Monitoring of Cementitious Materials: The Influence of Coating Materials, Engineered Science, 11 (2020) 66-75.

[3] Y.-F. Su, G. Han, T. Nantung, N. Lu, Novel methodology on direct extraction of the strength information from cementitious materials using piezo-sensor based electromechanical impedance (EMI) method, Construction and Building Materials, 259 (2020) 119848.

[4] Y.-F. Su, R.R. Kotian, N. Lu, Energy harvesting potential of bendable concrete using polymer based piezoelectric generator, Composites Part B: Engineering, 153 (2018) 124-129.

[5] L. Edery-Azulay, H. Abramovich, Piezoelectric actuation and sensing mechanisms—closed form solutions, Composite Structures, 64 (2004) 443-453.

[6] W.S. Na, J. Baek, A Review of the Piezoelectric Electromechanical Impedance Based Structural Health Monitoring Technique for Engineering Structures, Sensors, 18 (2018).

[7] S. Bhalla, C.K. Soh, Electromechanical Impedance Modeling for Adhesively Bonded Piezo-Transducers, Journal of Intelligent Material Systems and Structures, 15 (2004) 955-972.

[8] V.G.M. Annamdas, M.A. Radhika, Electromechanical impedance of piezoelectric transducers for monitoring metallic and non-metallic structures: A review of wired, wireless and energy-harvesting methods, Journal of Intelligent Material Systems and Structures, 24 (2013) 1021-1042.

[9] E. Ghafari, N. Lu, Self-polarized electrospun polyvinylidene fluoride (PVDF) nanofiber for sensing applications, Composites Part B: Engineering, 160 (2019) 1-9.

[10] Z.H. Liu, C.T. Pan, L.W. Lin, H.W. Lai, Piezoelectric properties of PVDF/MWCNT nanofiber using near-field electrospinning, Sensors and Actuators A: Physical, 193 (2013) 13-24.

[11] S.M. Damaraju, S. Wu, M. Jaffe, T.L. Arinzeh, Structural changes in PVDF fibers due to electrospinning and its effect on biological function, Biomedical Materials, 8 (2013) 045007.

[12] J. Zheng, A. He, J. Li, C.C. Han, Polymorphism Control of Poly(vinylidene fluoride) through Electrospinning, Macromolecular Rapid Communications, 28 (2007) 2159-2162.

[13] A. Lund, B. Hagström, Melt spinning of poly(vinylidene fluoride) fibers and the influence of spinning parameters on β-phase crystallinity, Journal of Applied Polymer Science, 116 (2010) 2685-2693.

[14] N. Soin, D. Boyer, K. Prashanthi, S. Sharma, A.A. Narasimulu, J. Luo, T.H. Shah, E. Siores, T. Thundat, Exclusive self-aligned β-phase PVDF films with abnormal piezoelectric coefficient prepared via phase inversion, Chemical Communications, 51 (2015) 8257-8260.

[15] G. Zhu, Z. Zeng, L. Zhang, X. Yan, Piezoelectricity in β-phase PVDF crystals: A molecular simulation study, Computational Materials Science, 44 (2008) 224-229.

[16] L. Li, M. Zhang, M. Rong, W. Ruan, Studies on the transformation process of PVDF from α to β phase by stretching, RSC Advances, 4 (2014) 3938-3943.

[17] S. Mishra, R. Sahoo, L. Unnikrishnan, A. Ramadoss, S. Mohanty, S.K. Nayak, Investigation of the electroactive phase content and dielectric behaviour of mechanically stretched PVDF-GO and PVDF-rGO composites, Materials Research Bulletin, 124 (2020) 110732.

[18] C.-W. Tang, B. Li, L. Sun, B. Lively, W.-H. Zhong, The effects of nanofillers, stretching and recrystallization on microstructure, phase transformation and dielectric properties in PVDF nanocomposites, European Polymer Journal, 48 (2012) 1062-1072.

[19] V. Sencadas, M.V. Moreira, S. Lanceros-Méndez, A.S. Pouzada, R. Gregório Filho, α- to β Transformation on PVDF Films Obtained by Uniaxial Stretch, Materials Science Forum, 514-516 (2006) 872-876.

[20] E. Ghafari, Polymer-based Piezoelectric Material and Device for Energy Harvesting and Sensing in Civil Infrastructure, Purdue University, Ann Arbor, 2018, pp. 102.

[21] H. Li, L. Wang, Y. Zhu, P. Jiang, X. Huang, Tailoring the polarity of polymer shell on BaTiO3 nanoparticle surface for improved energy storage performance of dielectric polymer nanocomposites, Chinese Chemical Letters, (2021).

[22] K. Shi, B. Chai, H. Zou, P. Shen, B. Sun, P. Jiang, Z. Shi, X. Huang, Interface induced performance enhancement in flexible BaTiO3/PVDF-TrFE based piezoelectric nanogenerators, Nano Energy, 80 (2021) 105515.

[23] E. Kabir, M. Khatun, L. Nasrin, M.J. Raihan, M. Rahman, Pureβ-phase formation in polyvinylidene fluoride (PVDF)-carbon nanotube composites, Journal of Physics D: Applied Physics, 50 (2017) 163002.

[24] Z. Jin, K.P. Pramoda, S.H. Goh, G. Xu, Poly(vinylidene fluoride)-assisted melt-blending of multi-walled carbon nanotube/poly(methyl methacrylate) composites, Materials Research Bulletin, 37 (2002) 271-278.

[25] M. Wu, L.L. Shaw, On the improved properties of injection-molded, carbon nanotube-filled PET/PVDF blends, Journal of Power Sources, 136 (2004) 37-44.